MICROBIAL AND CHEMICAL ENHANCEMENT OF IN-SITU CARBON MINERALIZATION IN GEOLOGICAL FORMATION

DOE Award Number: DE-FE0002389

Final Report

Reporting Period: 12/1/2009 – 5/31/2013

Columbia University

PI: Ah-Hyung Alissa Park

Tel: 1-212-854-8989, Fax: 1-212-854-7081, E-mail: ap2622@columbia.edu

Address: 918 S.W. Mudd Hall, MC4711

500 W. 120th Street, New York, NY 10027

Co-PI: J. Matter and K. Chandran

Date: December 15, 2013

DISCLAIMER* --

Table of Contents

ABSTRACT

Predictions of global energy usage suggest a continued increase in carbon emissions and rising concentrations of CO_2 in the atmosphere unless major changes are made to the way energy is produced and used. Various carbon capture and storage (CCS) technologies are currently being developed, but unfortunately little is known regarding the fundamental characteristics of CO_2-mineral reactions to allow a viable in-situ carbon mineralization that would provide the most permanent and safe storage of geologically-injected CO_2.

The ultimate goal of this research project was to develop a microbial and chemical enhancement scheme for in-situ carbon mineralization in geologic formations in order to achieve long-term stability of injected CO_2. Thermodynamic and kinetic studies of CO_2-mineral-brine systems were systematically performed to develop the in-situ mineral carbonation process that utilizes organic acids produced by a microbial reactor.

The major participants in the project are three faculty members and their graduate and undergraduate students at the School of Engineering and Applied Science and at the Lamont-Doherty Earth Observatory at Columbia University: Alissa Park in Earth and Environmental Engineering & Chemical Engineering (PI), Juerg Matter in Earth and Environmental Science (Co-PI), and Kartik Chandran in Earth and Environmental Engineering (Co-PI). Two graduate students, Huangjing Zhao and Edris Taher, were trained as a part of this project as well as a number of graduate students and undergraduate students who participated part-time. Edris Taher received his MS degree in 2012 and Huangjing Zhao will defend his PhD on Jan. 15th, 2014. The interdisciplinary training provided by this project was valuable to those students who are entering into the workforce in the United States. Furthermore, the findings from this study were and will be published in referred journals to disseminate the results. The list of the papers is given at the end of the report for reference.

PROJECT OBJECTIVES

In-situ carbon mineralization is one of the best storage pathways for geologic sequestration in terms of its long-term stability. However, there has been very little systematic effort in the study of the carbonation of non-carbonate minerals including Mg-bearing minerals such as serpentine, and some reported results are contradictory among CO_2 sequestration researchers. Particularly, the fate of the dissolving species (i.e. Mg, Si and Fe) and the process of magnesium carbonate precipitation in the presence of complex ions have been disputed by many researchers, but no concrete answers have yet been suggested. Thus, this project aimed to provide the knowledge basis for in-situ CO_2-mineral-brine interaction for geologic sequestration. Furthermore, a microbial system that produces weak acids was developed in order to chemically enhance the in-situ mineral

dissolution and, in turn, to achieve faster carbon mineralization kinetics as illustrated in Figure 1. The proposed project was also designed to provide important research experience for both graduate and undergraduate students who will be faced with the challenge of implementing and deploying CCS technologies.

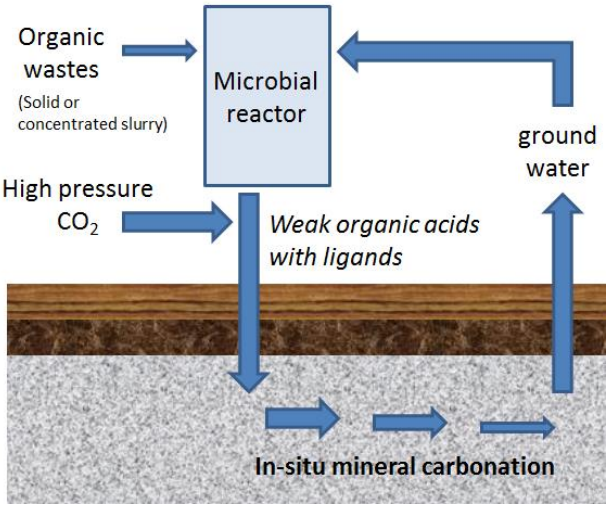

Figure 1. Overall schematics of the developed microbial and chemical enhancement of in-situ carbon mineralization scheme

SPECIFIC QUESTIONS

The sequestration of CO_2 generally involves three steps: capture, transportation, and storage.[1] Regardless of the method of carbon capture, the separated CO_2 must be transported to disposal facilities. Most current large-scale carbon sequestration projects utilize disposal based on injecting the captured CO_2 into geological formations. This process is attractive because the initial disposal cost is low.[1] Despite initial economic advantages, geological sequestration is not without potential problems related to leakage and accidental release of the sequestered gas.[2] To address this issue, researchers are now investigating the fate of injected CO_2 in geologic formations as well as working on the issue of long-term monitoring of injection sites.

CO_2 is the anhydrous form of carbonic acid and, therefore, can be used to displace weaker acids such as silicic acid. The formation of carbonates from silicate minerals, which thermodynamically bind CO_2, is a well-known process called mineral weathering. In many instances these carbonates dissolve in water, but some, such as Mg or Ca-carbonates, are remarkably stable as solids. For example, serpentine can react with CO_2 and form thermodynamically stable mineral carbonates.[3]

$$Mg_3Si_2O_5(OH)_4 + 3CO_2 \rightarrow 3MgCO_3 + 2SiO_2 + 2H_2O + 64\ kJ\ mol^{-1}CO_2$$

The total accessible deposits of the Mg-bearing minerals, including serpentine ($Mg_3Si_2O_5(OH)_4$), are estimated to significantly exceed the worldwide coal reserves.[3,4] However, the reaction between mineral and CO_2 is very slow in nature, and thus, the portion of carbon storage by in-situ mineralization has been estimated to be very limited in geological sequestration.

Researchers including the PI's group worked on the enhancement of mineral carbonation process as an ex-situ process.[5-9] Most of the prior studies focused on the pretreatment of minerals to increase the overall conversion, including heat treatment and

wet-attrition grinding of Mg-silicate minerals.[5,8-9] These methods, however, were highly energy intensive and cannot be applied to geologic sequestration.

Preliminary to this project, the PI advised a group of undergraduate students for their senior design project to develop a biological system by modifying her pH swing process that chemically enhances the mineral dissolution and carbonation processes. There are strains of bacteria and fungi that enhance dissolution of Mg-silicates. When they are dissolved, organic acids create protons that attach to the mineral surface at the oxygen sites, thus making the metal-oxygen bond weaker and speeding up dissolution. The rate of mineral dissolution is also affected by organic ligands' affinity towards Mg forming complexes. The cation-oxygen bond grows weaker when metal-organic complexes form at the point at which the solid meets the solution, making the dissolution reaction occur faster.[10] The main acid formed by bacteria is 2-ketogluconic acid, and other acids include citric and oxalic acids, which are formed by fungi. Generating gluconate and 2-ketoglutarate is a process that many bacteria have in common and which generates energy.[11]

The organic acids such as gluconic acid can also be produced from various organic wastes via microbial process. The Co-PI, Chandran, has already developed an optimized process of pre-fermentation and acid-phase digestion to produce volatile fatty acids for full-scale adaptation by the City of New York in 2002,[12] which is the same process to be employed in this proposed study. For such microbial systems (e.g., Figure 3), the different microbial concentrations (X1-X5) can be quantified via molecular genetics approaches and the different processes can be described using biokinetic and metabolic modeling.

Based on these preliminary data and interdisciplinary expertise within the project team, the following key scientific and engineering questions were addressed for this research:

- What are the optimum reaction conditions of the microbial production of organic acids?
- What are the effects of organic acids on the dissolution kinetics of Mg-bearing minerals?
- What are the effects of reaction temperature, pH, and pore sizes of the geologic formations on the crystal structure and chemical compositions of the mineral carbonates?
- What would be the tangible environmental benefit of the in-situ carbon mineral sequestration?

The following sections summarize the main findings from this project in detail.

1. Anaerobic Digestion

1.1. Anaerobic Digestion of Glucose

Glucose, which is a completely soluble material, was used as the substrate for the microbial reactor system, and Mix Culture Biotechnology (MCB) was used for the production of different kinds of chelating agents. MCB has many advantages, like utilizing complex wastes as feed, no need of sterile operation, low energy demand and simple process control. The main drawback is the production of various chelating agents simultaneously instead of a specific agent. Figure 2 shows the metabolic network fermenting microorganism and possible products.[13]

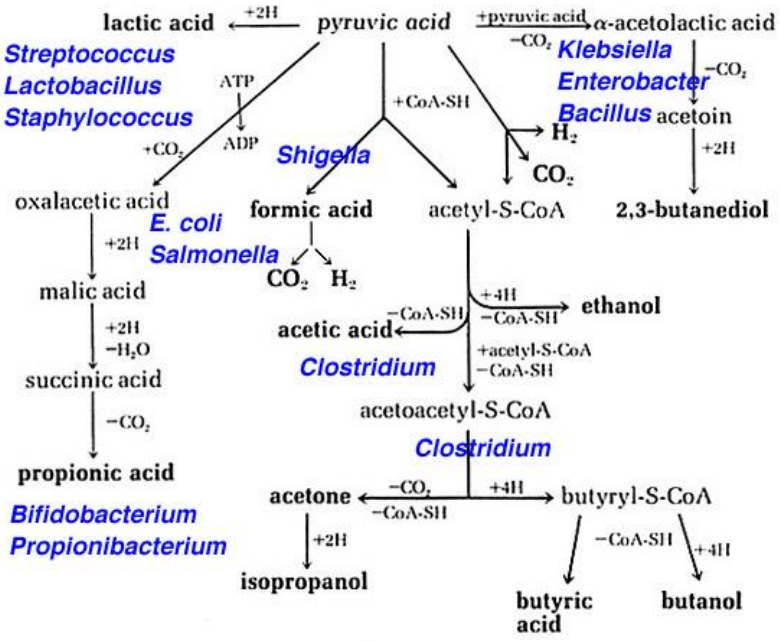

Figure 2: Metabolic network of the virtual carbohydrate fermenting microorganism

A 3 L sequencing batch reactor (SBR) reactor was employed to perform anaerobic digestion experiments using glucose. The total fermentation time was 24 hours and at the end of each batch experiment 2 L of broth was pumped out from the reactor and the rest (1 L) was kept as inoculums for the next batch. The reactor was filled again with 2 L of fresh medium and a cycle was started. The cultivation medium was prepared using the following: 10 g/L of glucose, 1.8 g/L of NH_4Cl, 1.95 g/L of KH_2PO_4, 0.73 g/L of NaCl, 0.33 g/L of Na_2SO_4 0.33, 0.3 g/L of $MgCl_2$ and 7 ml of trace elements. The NH_4Cl requirement was calculated assuming that 50% of glucose is consumed in the anaerobic reaction and biomass can be represented as $C_1H_{1.4}O_{0.4}N_{0.2}$.

$$6 * 0.056 * 0.2 * 50\% = 0.033\ mol\ N\ \ or\ \ 0.033\ mol * 53.5\frac{g}{mol} NH_4C = 1.8\ g\ NH_4Cl$$

The makeup of the trace elements is given in Table 1. The pH of the system was automatically controlled and maintained at 7 using a buffer solution of 1 M sodium bicarbonate and 1 M sodium hydroxide. Experiments were continued for 1 month. All laboratory analyses were conducted according to the Standard Methods for Examination of Water and Waste water. The Volatile Fatty Acid (VFA) speciation and their concentrations were analyzed using an Ion Chromatograph (IC). Samples were filtered through a 0.45 μm filter paper prior to the testing of soluble COD. Microbial samples were stored every four days for the further analysis of the microbial consortia in the reactor.

Table 1: Trace elements of acidification process

Component	Concentration (g/L)
$FeSO_4$	0.62
$CaCl_2$	0.12
H_3BO_4	0.02
Na_2MoO_4	0.02
$ZnSO_4$	0.64
$CoCl_2$	0.12
$CuCl_2$	0.44
$MnCl_2$	0.5
$NiCl_2$	0.1
EDTA	10

Since biomass is not fully soluble in water, the biomass based COD was theoretically calculated based on the following formula. The results were summarized in Table 2.

$$1C_1H_{1.4}O_{0.4}N_{0.2} + 1O_2 \ \rightarrow \ 1CO_2 + 0.8H_2O + 0.2NH_3$$

$$\Rightarrow COD_X = \frac{1mol\ O_2}{1\ mol\ X} = \frac{32\ g\ O_2}{22.6\ g\ X} = 1.416\frac{g\ O_2}{g\ X}$$

Therefore, $X_{gram\ biomass} = \frac{COD_{total} - COD_{Souluble}}{COD_X}$.

Table 2: Total COD, soluble COD, ammonia and theoretical biomass concentrations (g/L)

day: gr/L	TCOD effluent	SCOD effluent	NH3 effluent	N/TCOD	Biomass based on COD
0	7.14	4.34	0.46	0.06	1.98
1	4.07	3.01	0.35	0.09	0.75
2	3.01	1.74	0.32	0.11	0.89
5	2.74	2.01	0.34	0.13	0.52
6	4.07	2.41	0.39	0.10	1.18
7	4.87	3.34	0.42	0.09	1.08
8	3.54	2.41	0.51	0.15	0.80
10	6.14	4.34	0.49	0.08	1.27
12	3.41	2.74	0.37	0.11	0.47
16	3.27	2.61	0.38	0.12	0.47
20	3.01	2.47	0.38	0.13	0.38
22	3.07	2.54	0.36	0.12	0.38

Table 3: COD values of fatty acids (mg-O_2/mg-FA)

Name	Furmula	MW	COD
Succinate	C4H6O4	118.1	0.95
Lactate	C3H6O3	90.1	1.07
Acetate	C2H4O2	60	1.07
Propinate	C3H6O2	74.1	1.51
Butyrate	C4H8O2	88.1	1.82
Valerate	C5H10O2	102.1	2.04

Table 4: Fatty acid concentrations (mg/L)

mg/L : day	Succinate	Lactate	Acetate	Propinate	Butyrate	Valerate	Total COD	SCOD	Accuracy
0	95.95	81.50	55.43	419.12	1296.98	0.00	3225.91	4340.00	0.74
1	77.94	64.74	44.22	0.00	1018.78	106.88	2258.02	3006.67	0.75
2	46.72	38.57	0.00	0.00	630.79	56.06	1345.20	1740.00	0.77
5	0.00	51.27	35.12	0.00	743.95	49.94	1544.93	2006.67	0.77
6	57.67	0.00	0.00	254.89	696.07	78.55	1864.12	2406.67	0.77
7	92.78	76.83	52.77	0.00	1164.86	127.50	2601.41	3340.00	0.78
8	53.25	44.17	30.38	235.35	723.42	38.38	1877.70	2406.67	0.78
10	92.04	76.55	52.42	406.42	1192.35	130.24	3269.83	4340.00	0.75
12	58.34	0.00	33.19	257.63	775.60	81.45	2054.64	2740.00	0.75
16	0.00	0.00	35.73	277.21	778.07	50.34	1972.73	2606.67	0.76
20	52.08	43.12	0.00	229.44	714.30	72.23	1886.53	2473.33	0.76
22	49.23	40.87	31.24	217.22	750.54	44.18	1904.95	2540.00	0.75

Since the glucose concentration in the feed was 11.6 g/L COD, the same concentration of the total COD in the effluent was expected once the system reached a steady state condition. However, the measured total COD in the effluent was approximately 30% of the predicted value. Acidification is a fast process and the time required to exhaust glucose in our system should not be longer than 6 hours. As described in the acidification pathway (Figure 2), glucose is first metabolized to two moles of pyruvate and two moles of ATP are released. The produced pyruvate then goes through other cycles and is consumed as a substrate to produce VFA, other metabolites, hydrogen and carbon dioxide as by-products. Because of high HRT, after the exhaustion of glucose the significant amount of produced metabolites will be utilized as substrates by methanogenesis and generates carbon dioxide and hydrogen. Therefore, it can be concluded that the uncounted part of COD has been removed from the reactor in forms of hydrogen and carbon dioxide. The concentrations and species of produced fatty acids were determined using an IC. Further, based on the COD value of each fatty acid listed in Table 3, an overall COD balance was conducted to determine the measurement accuracy of the IC. The results were summarized in Table 4. From the IC results, it was found that the measured fatty acids contain 75% of soluble COD. The rest of 25% might be either other metabolites like alcohols which cannot be measured by the IC.

In Figure 3, the mean concentrations of produced VFAs were presented. The main VFA product was butyrate (70% of the total VFAs). Butyrate was followed by propionate which was also produced in a significant quantity (15% of the total VFAs). Other VFAs were found in much lower concentrations.

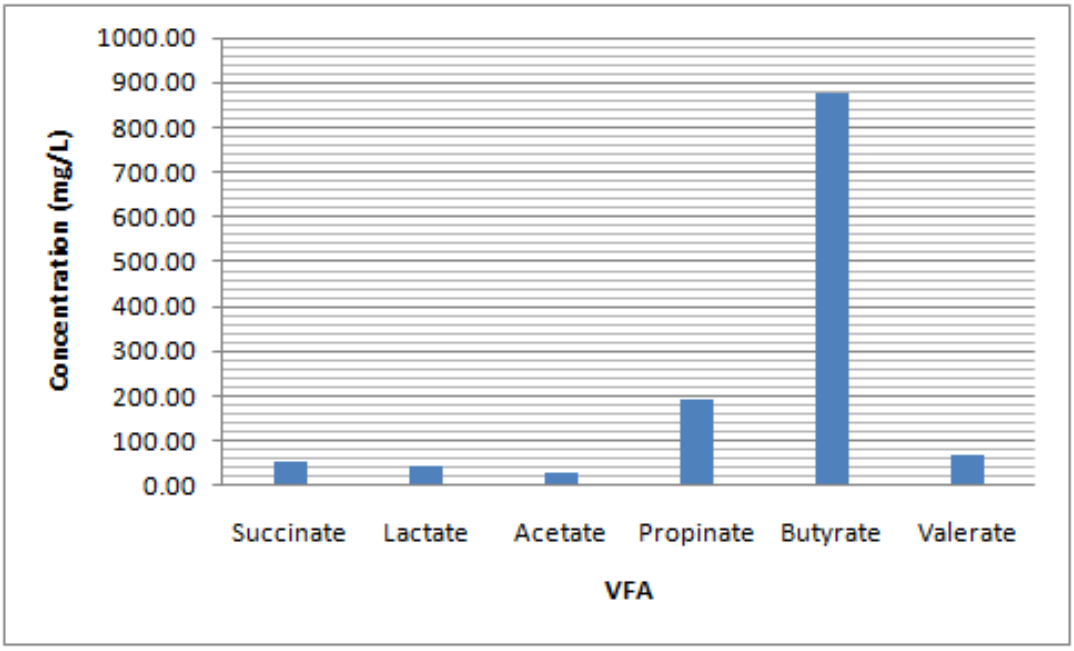

Figure 3: Mean concentrations of VFAs produced from glucose

1.2. Anaerobic Digestion of Food Waste

Figure 4 shows the proposed reaction scheme of the anaerobic digestion of food waste. Six distinct processes are included in the anaerobic digestion of food waste. They are hydrolysis of biopolymers, fermentation of amino acids and sugars, anaerobic oxidation of long chain fatty acids and alcohols, anaerobic oxidation of intermediary products such as volatile acids (with the exception of acetate), conversion of acetate to methane and conversion of hydrogen to methane.[14] In general methane (or hydrogen) is the final product of the anaerobic digestion of food waste. However the process can be controlled to produce fatty acids by tuning experimental conditions (e.g., reaction time).

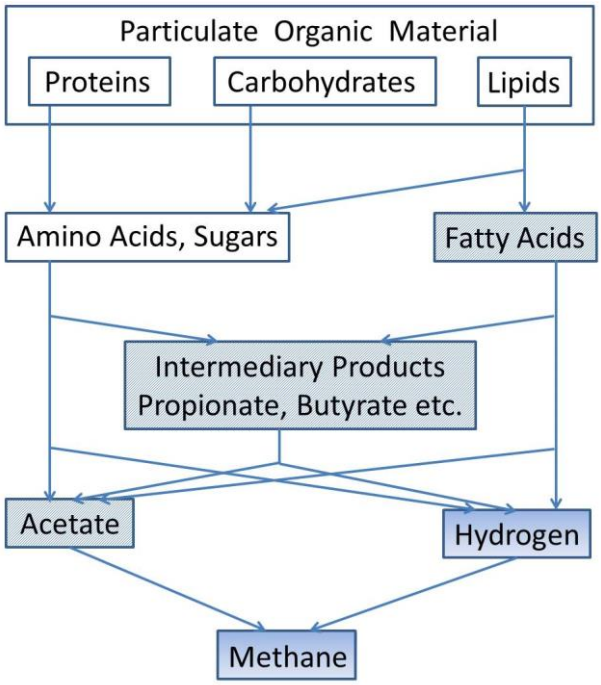

Figure 4: Proposed reaction scheme of the anaerobic digestion of food waste

Food waste from Columbia University's cafeteria was used as substrate for the microbial reactor system. Experiments were executed in a 6 L SBR instead of a 3 L SBR at 25 °C. However, the same MCB and cultivation medium were used for anaerobic digestion of food waste, and the pH was automatically controlled and maintained at 7 using buffer solution of 1 M sodium bicarbonate and 1M sodium hydroxide. After finishing the first batch, the experiment was repeated to examine the achieved pattern.

In both experiments, acetate and propionate were the main produced fatty acids (Figure 5). After 10 days of reaction, with hydraulic retention time (HRT) of 2 days, all measured fatty acids reached their maximum concentration and a reduction in fatty acids

was perceived over time. In both experiments, 60-75% of soluble COD was found in the measured fatty acids. COD and N/C ratio remained constant during the reaction.

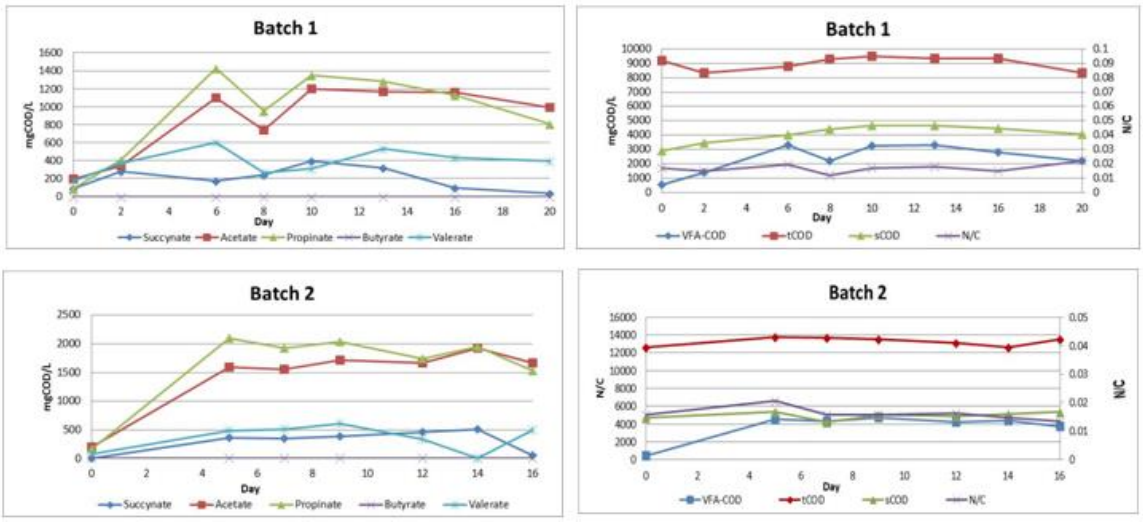

Figure 5: Measured concentrations of components vs. time

It is possible to get a more specific product than others by controlling the operational variables, e.g. pH, temperature, composition of substrate, feed pattern and electron acceptable availability. However, in this study, our effort was focused on the effect of HRT on the final products.

From Figure 6 and Figure 7, it was found that maximum yield was achieved at 2 days and 4 days HRT. But the maximum production rate was observed at 1 day and 2 days HRT. Considering the yield and production rate together, the optimum HRT should be 2 days.

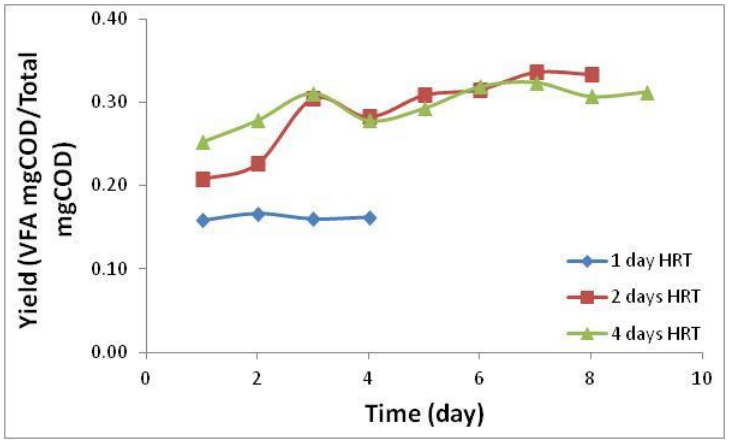

Figure 6: Yield of the total produced VFAs vs. hydraulic retention time

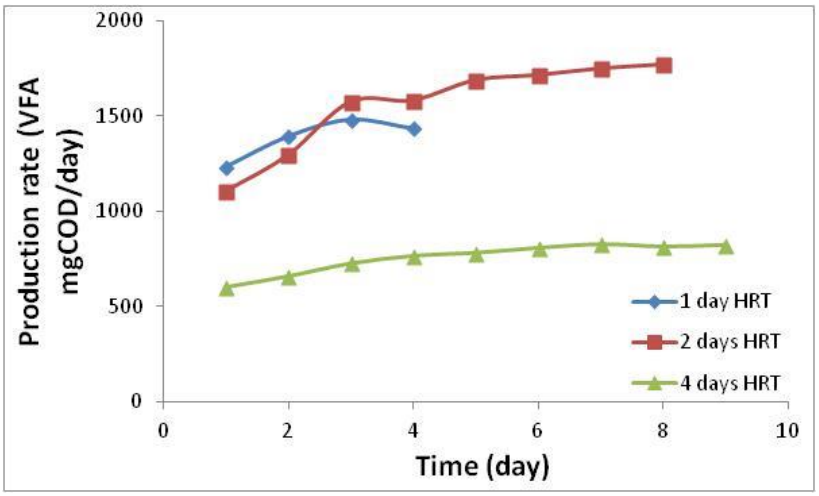

Figure 7: Production rate vs. retention time

Figure 8 shows the yield of total VFAs and each species in 2 days HRT test. 30% of the total substrate was converted to VFAs. Acetate and propionate were the dominant products in the anaerobic digestion of food waste. It was found that soluble COD was around 38% of the total COD. Since not all the soluble COD can be converted to VFAs, there is a difference of 8% between the measured soluble COD and total produced VFAs. Soluble COD can also be converted to other organic components, for example alcohols which were not measured in the tests.

Based on all the conducted experiments and results, it was found that the optimum hydraulic retention time is 2 days for the process of anaerobic digestion of Columbia cafeteria's food waste. In the downstream section, produced fatty acids can be easily separated from the solid waste by filters and used as chelating agents in carbon mineralization process. The separated solid waste can either be hydrolyzed and reused as feed or directly used as fertilizer.

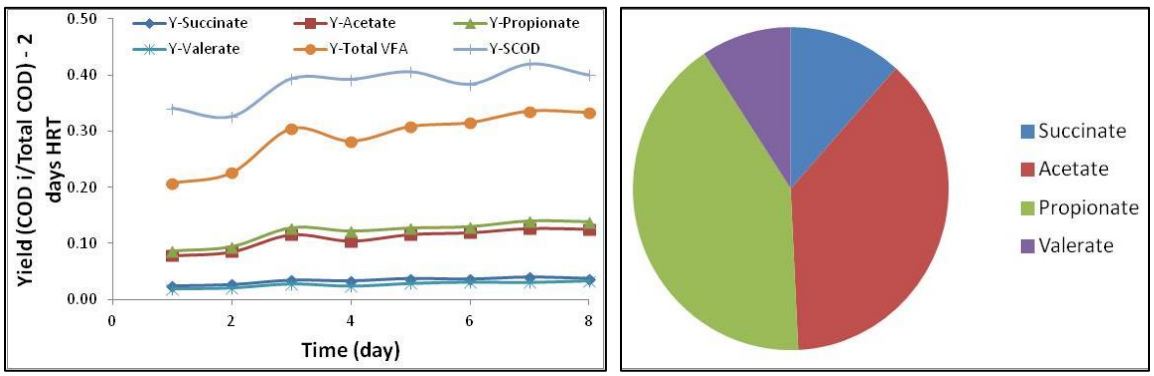

Figure 8: Yield of total VFAs (left) and each species in 2 days HRT test (right)

2. Thermodynamic Modeling of CO_2-Mineral-Water System

Thermodynamic modeling of CO_2-mineral-water system was carried out using software called Visual MINTEQ. Visual MINTEQ is a Windows version of MINTEQA2 ver 4.0, which was released by the United States Environmental Protection Agency (U.S. EPA) in 1999. It is the most widespread chemical equilibrium model for thermodynamic calculations such as metal speciation and solubility equilibria, for natural waters. It is renowned for its stability. Visual MINTEQ is capable of (Gustafsson, 2004):

- **Ion speciation using equilibrium constants from the MINTEQA2 database, which has been updated using the most recent NIST data to contain > 3000 aqueous species and > 600 solids**
- **Solubility calculations involving solids phases**
- Adsorption calculations with five surface complexation models (Diffuse Layer, Constant Capacitance, Triple Layer, Basic Stern and Three Plane), with the 1-pK or 2-pK formalisms, and with the CD-MUSIC concept
- Ion-exchange calculations using the Gaines-Thomas formalism
- Calculations with redox couples and **gases (e.g. CO_2)**
- Metal-humic complexation can be simulated using either the Gaussian DOM or the Stockholm Humic Model.
- **Sweep runs in which one parameter is varied, e.g. pH** or the total concentration of component
- Titrations in which a titrant with a given composition is added in steps to the original solution
- Presentation of results from Visual MINTEQ runs on separate output tables; export of results to EXCEL
- Management of Visual MINTEQ's thermodynamic databases from within the program

The highlighted functions are the ones used most frequently in this study. Many of these functions were more closely related to the natural water system with a low ionic strength. For high concentration chemical systems, the model should be used with caution.[15]

First, the effect of the CO_2 partial pressure on the dissolution of chrysotile was investigated. Chrysotile, which is an important mineral polymorph of serpentine, was selected as the mineral phase due to the availability of thermodynamic data. The concentration of chrysotile was set as infinite and the simulation was carried out at 25 ºC. Three CO_2 partial pressures were selected to mimic the atmospheric condition (385 ppm), the flue gas condition (0.15 atm), and pure CO_2 stream (1 atm). As shown in Figure 9, a

higher partial pressure of CO_2 resulted in a lower pH, and this led to increased dissolution of chrysotile. Although the dissolution of CO_2 in water can generally reach much lower pH (~3.5) conditions, the presence of excess basic mineral, chrysotile, resulted in final pH of given aqueous systems to be greater than 6.7 even at P_{CO2} = 1 atm. In these cases, pH was calculated based on mass and charge balances.

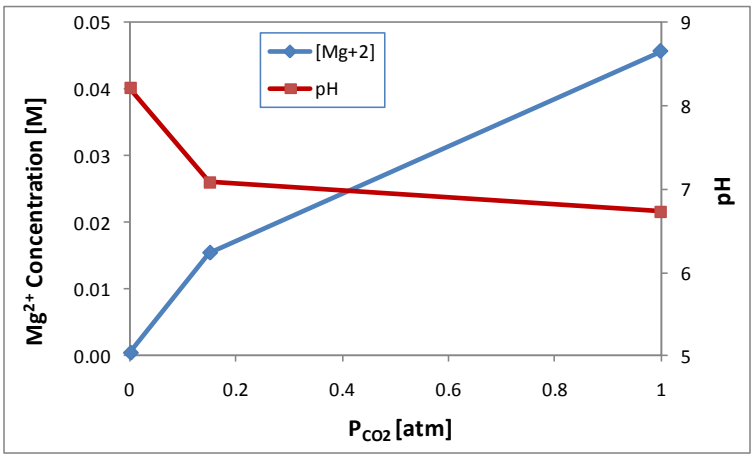

Figure 9: Effect of partial pressure of CO_2 on chrysotile dissolution at 25 ºC

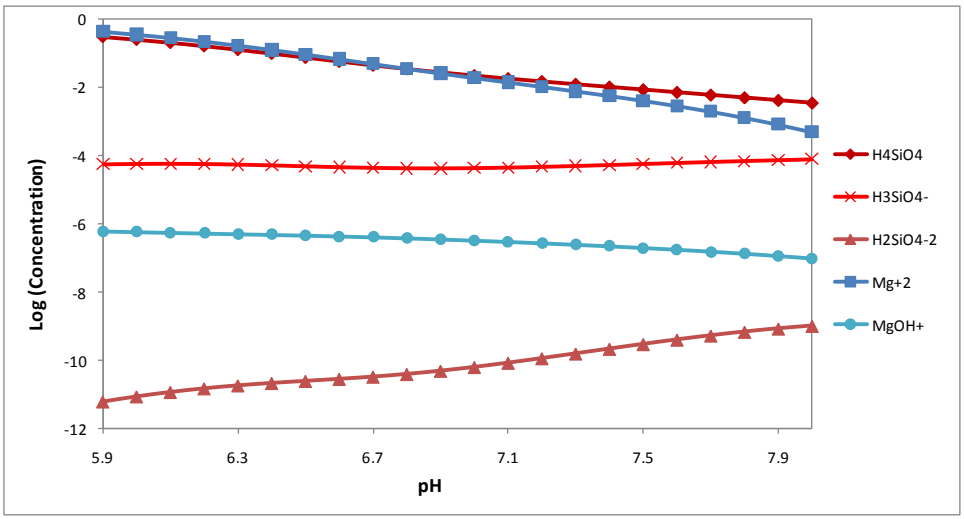

Figure 10: Equilibrium concentrations of dissolved aqueous species of chrysotile at P_{CO_2} =1 atm and 25 ºC.

Next, the effect of pH on the dissolution of chrysotile was investigated under fixed pH conditions. Fixed pH conditions simulate dissolution studies that would be performed with buffers. According to the results of thermodynamic calculations given in

Figure 10, when excess amount of chrysotile is dissolved in aqueous phase, the extraction of Mg from the mineral matrix is greater at low pH conditions in both Mg^{2+} and $MgOH^{+}$ forms. On the other hand, the dissolution of silica layers represented by Si-species such as H_4SiO_4, H_3SiO^{4-} and $H_2SiO_4^{2-}$ was suppressed at low pH conditions. The results shown here are only for the pH range from 5.9 to 8, because very low and very high pH conditions would result in ionic strength greater than 1 M.

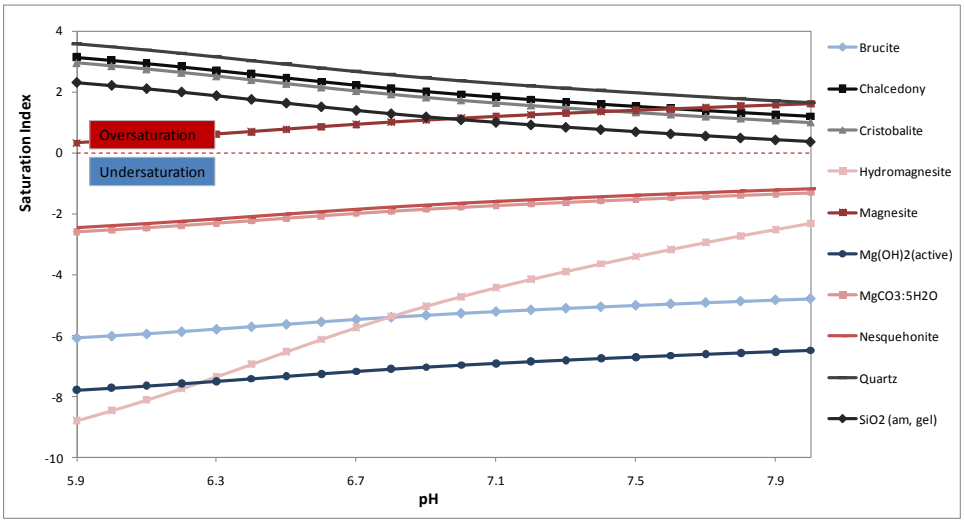

Figure 11: Saturation indices of different aqueous species in chrysotile-water-CO_2 system at P_{CO2} =1 atm and 25 ºC.

Finally, saturation indices (SI) of different aqueous species in the presence of chrysotile at P_{CO2} =1 atm and 25 ºC were determined and the results are given in Figure 11. SI is defined as log (IAP/K_{sp}), where IAP is the ion activity product and K_{sp} is the temperature-corrected solubility constant. If SI > 0, it means oversaturation. By contrast, if SI < 0, it means undersaturation and under-saturated aqueous species will remain in water phase while the oversaturated species would precipitate out as solid phases. Within the given pH range, SI of most of Mg-species were increased as pH increased, however, they were still undersaturated except magnesite ($MgCO_3$). In the case of Si-species, quartz, SiO_2 (both amorphous and gel), chalcedony and cristobalite were all oversaturated even at the highest given pH.

3. Procurement and Analysis of Minerals

Cedar Hill antigorite from Albany Research Center was selected for the study. They were milled to minus 200 mesh (< 75 μm). A comprehensive protocol was developed for the preparation of mineral samples for the subsequent kinetic studies,

because the fines (< 5 μm) present in mineral samples would lead to unrepresentatively high initial mineral dissolution rates due to extremely high surface to volume ratio. Thus, it is important to remove fines prior to the kinetic studies. Unfortunately, most of the prior studies performed in this field directly used the raw mineral samples, and as a result, the collected kinetic data were not consistent.

The raw mineral sample was first placed in a 10 μm sieve manufactured by W.S. Tyler. The sieve containing the mineral sample was covered with a solid cap and was shaken in an ultrasonic bath filled with deionized (D.I.) water for 5 minutes to wash out the fines. At the end of washing cycle, D.I. water was replaced by fresh D.I. water and the washing step was repeated. This process was repeated five times, and therefore, the total washing time was 25 minutes. A vacuum oven was used to dry the cleaned minerals.

LS™ 13 320 Series Laser Diffraction Particle Size Analyzer manufactured by Beckman Coulter was used to evaluate the particle size and particle size distribution. This instrument is capable of measuring particle sizes from 0.4 μm to 2000 μm. Laser diffraction is based on Fraunhofer and Mie theories. Fraunhofer theory is applicable for spherical, non-porous and opaque particles such that all the particles diffract the light with the same efficiency. While the Fraunhofer theory is applicable for large particles, it is more appropriate to use Mie model for small particles since it accounts for both diffraction and diffusion of the light around the particle in its medium. The observation of the diffraction pattern at finite distance is done through a lens placed between the laser source and the detector. JEOL Scanning Electron Microscope was used to obtain the morphological structures of the mineral samples, while NOVA 2200e BET analyzer was used to determine the surface area and pore size distributions of the mineral samples.

Based on the above method, most of the fines were successfully removed from the antigorite sample leaving less than 0.01% of fines in volume as illustrated in Figures 11 and 13. As expected, after the washing process, the average particle size was increased and the specific surface area was decreased (Tables 5). As shown in Figure 12, the XRD spectra of raw and washed antigorite were slightly different. The chemical composition of raw and cleaned antigorite minerals were analyzed by X-ray fluorescence (XRF) technology. Table 6 shows the results.

Table 5: Particle sizes and surface areas of raw and cleaned antigorite minerals

Sample type	Mean diameter (μm)	Surface area (m^2/g)
Raw antigorite	23.63	6.44
Cleaned antigorite	45.66	3.00

Table 6: Chemical composition of raw minerals and cleaned minerals

Mineral Description	Raw Antigorite	Cleaned Antigorite
SiO2 (%)	37.2	37.1
Al2O3 (%)	0.36	0.36
Fe2O3 (%)	7.62	7.80
MgO (%)	40.5	40.5
CaO (%)	0.15	0.14
Na2O (%)	0.06	0.06
K2O (%)	0.01	0.02
TiO2 (%)	< 0.01	0.02
P2O5 (%)	< 0.01	< 0.01
MnO (%)	0.09	0.09
Cr2O3 (%)	0.40	0.47
V2O5 (%)	< 0.01	< 0.01
LOI (%)	14.8	13.1
Sum (%)	101.2	99.6

(LOI: Loss on Ignition, measured as the weight loss after 1 hour at 1000^{o}C, in argon.)

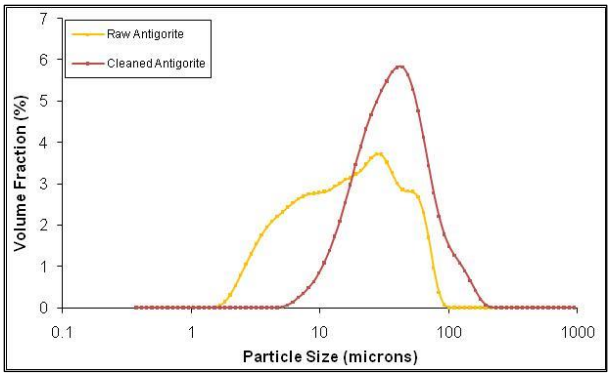

Figure 11: Particle size distribution of Cedar Hill Antigorite

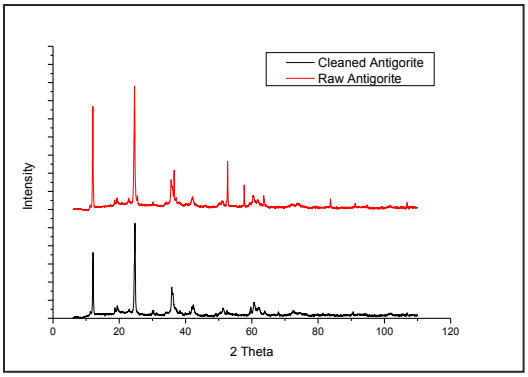

Figure 12: XRD results of Cedar Hill Antigorite

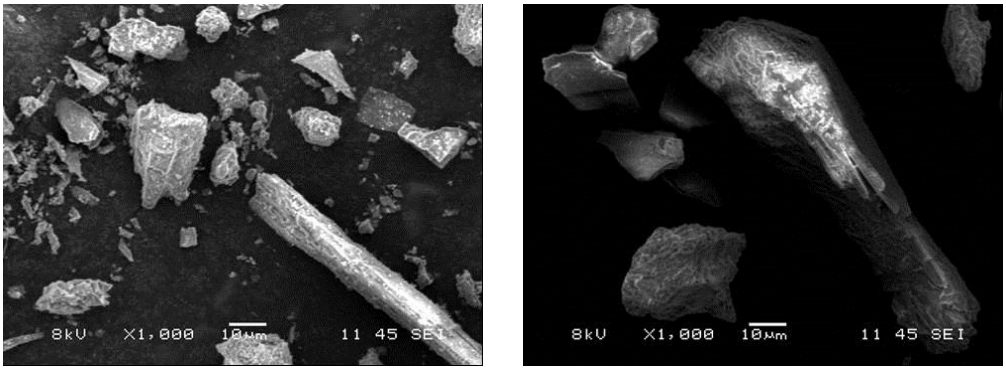

Figure 13: SEM photos of Cedar Hill Antigorite
(Left: Raw Antigorite and Right: Cleaned Antigorite)

4. Dissolution of Antigorite

Most of the reaction models developed for the dissolution of Mg-bearing minerals do not consider the role of ligands in mineral dissolution. In the absence of chelating agents, protons react with minerals at the surface and produce Mg^{2+} and silicic acid as shown in Figure 14 (left). This is how nature weathers silicate minerals and this process is very slow. In the surface reaction model, ligands, protons and Mg-targeting ligands react with minerals at the surface and make Mg^{2+}, Mg-complexes and silicic acid (Figure 14 (right)). This process is much faster than the surface reaction rate without the ligands. However, as the outer layer of the minerals is dissolved, a diffusion limiting Si-rich layer is formed. Therefore, the mineral dissolution rate would be limited by the mass transfer through the Si-rich layer rather than the surface reaction rate.

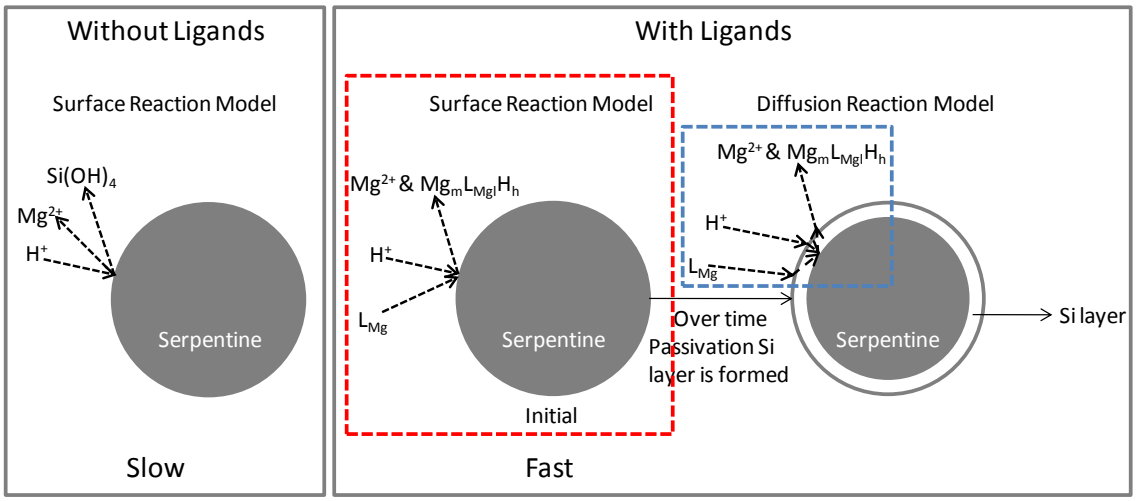

Figure 14: Proposed reaction models

In this project, surface reaction models (with or without chelating agents) were studied. The reactor setup to be used for the kinetic studies is shown in Figure 15. This reactor consists of a syringe pump instead of a batch mixing unit that was generally used in the prior work in literature. The filter holder is modified to accommodate a thin layer of mineral samples to create a differential bed reactor. This is to capture the fast reaction kinetic during the first few minutes of the mineral dissolution. Also, the application of the differential bed reactor will allow the use of the solvents without adding buffers since the thin layer of the mineral samples would be always in contact with the stream of fresh solvent.

Differential bed reactors are commonly used for measuring the rate of heterogeneously catalyzed reactions, and have features that make them attractive for mineral dissolution as well. They are characterized by a very short bed, containing a small amount of sample. The fluid residence time in the bed is short compared to the reaction rate, ensuring the liquid properties are constant across the bed and that the reacting species are not significantly depleted over the bed length. In the case of mineral dissolution, this short residence time would ensure that the solution pH does not change appreciably, removing the need for buffering or pH adjustment.

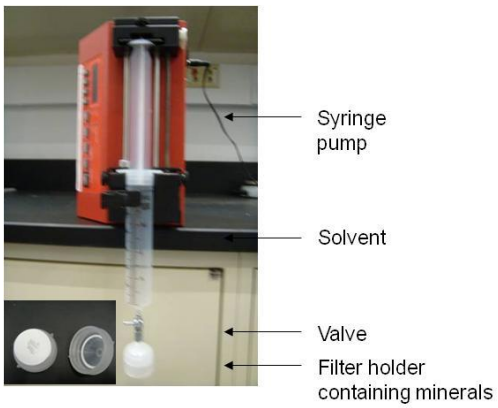

Figure 15: Differential bed reactor

For each experiment, 60 ml of the solvent containing a given chelating agent flowed through a bed of 100 mg of mineral sample at a rate of 10 ml/min. The total reaction time was 6 minutes and 4 filtrate samples were collected with a sampling interval of 5 seconds at the beginning of the experiment. The sampling rate was reduced to 10 seconds per sample for the latter part of the experiments. The elemental concentrations of Mg in the liquid samples will be analyzed using the inductively coupled plasma (ICP).

The addition of Mg-targeting chelating agents to the aqueous mineral system is expected to increase the extent of mineral dissolution. The effects of various chelating

agents, which were produced via the process of anaerobic digestion, were experimentally studied. 0.01 M sodium acetate, 0.01 M sodium propionate, 0.1 M sodium butyrate, 0.01 M valeric acid, 0.01 M sodium lactate and 0.01 M sodium succinate solvents were prepared. The solvents were adjusted pH to 2 and 5 with 70% nitric acid or 50 wt% sodium hydroxide.

At pH 2, valerate is the most effective chelating agent for the antigorite dissolution compared to acetate, propionate, butyrate, lactate and succinate at the same concentration. Propionate is the least effective chelating agent (Figure 16). At pH 5, valerate continues to be more effective than other chelating agents. At pH 5, however, succinate is a little better than acetate in facilitating antigorite dissolution.

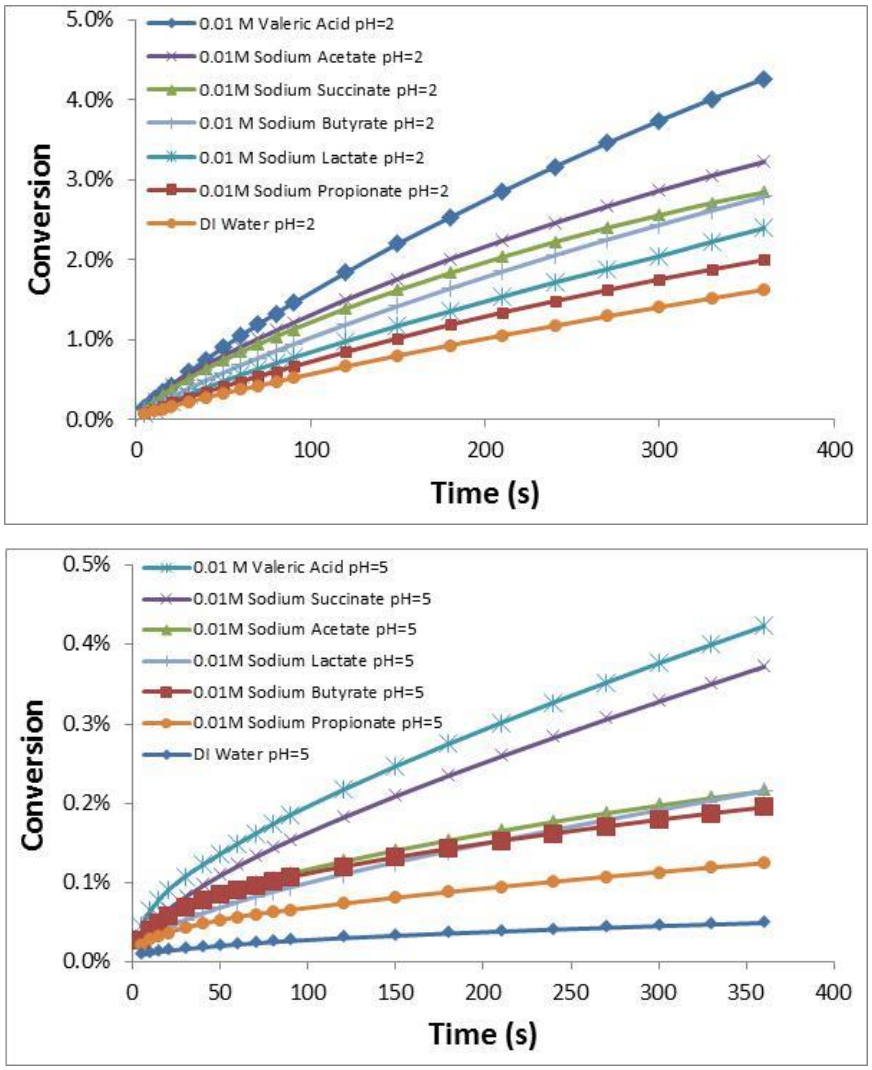

Figure 16: Effects of various chelating agents on antigorite dissolution at pH 2 (top) and 5 (bottom)

Figure 17 shows the activities of acetate$^-$, propionate$^-$, butyrate$^-$, valerate$^-$, lactate$^-$ and succinate^{2-} in their 0.01 M solution under various pH conditions. Activities of acetate$^-$, propionate$^-$, butyrate and valerate$^-$ are similar under various pH conditions. At low pH acetate has a higher activity than succinate, so acetate works better than succinate. At high pH, they have similar activities, and it was found that succinate was better than acetate because succinate can make stronger and more stable Mg complexes than acetate. The reason for valerate's effectiveness is not very well understood. Moreover, valerate is a rare chemical and there is lack of information of valerate compared to others. The stability constant of Mg-valerate complex is not known. Table 7 shows the properties of various chelating agents.

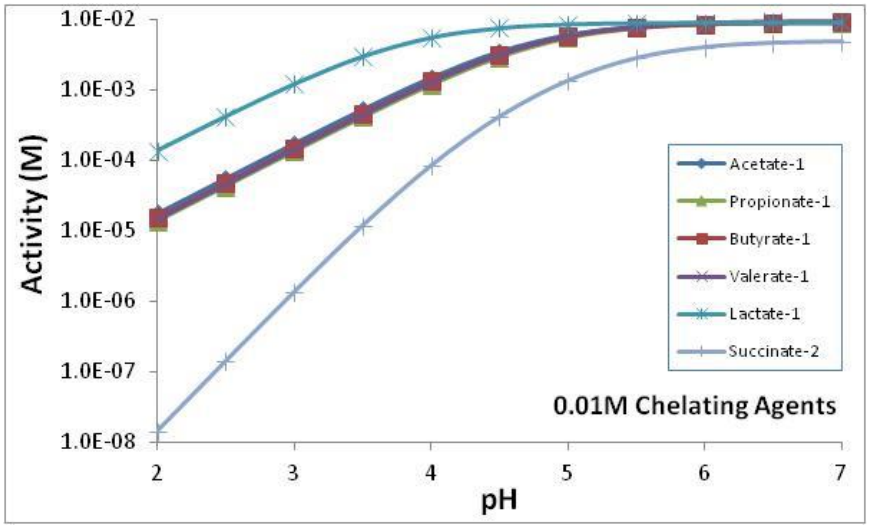

Figure 17: Activities of effective anions in their 0.01 M solution under various pH levels

Table 7: Properties of various chelating agents (β = stability constant)[16]

Chelating agent	Molecular Formula	Complex	Logβ
Acetate	CH_3COO^-	ML^-	0.51
Propionate	$CH_3CH_2COO^-$	ML^-	0.54
Butyrate	$CH_3CH_2CH_2COO^-$	ML^-	0.53
Valerate	$CH_3CH_2CH_2CH_2COO^-$	ML^-	–
Lactate	$CH_3CH(OH)COO^-$	ML^-	0.93
Succinate	$(CH_2COO)_2^{2-}$	ML/MHL^+	1.2

Most previous serpentine dissolution studies were focused on using strong acids to dissolve serpentine. Table 8 shows some published kinetic data and experimental conditions. The main issue of the high concentration strong acid serpentine dissolution process is its high energy consumption. Large amounts of base will be required to obtain the carbonates after dissolution. For this reason, researchers are looking for chelating agents that can enhance the rate of serpentine dissolution at higher pH (>2). With chelating agent enhanced dissolution, it is recognized that the total dissolution rate is the sum of proton-promoted dissolution rate and the ligand-promoted dissolution rate.[18, 19]

Table 8: Activation energy for serpentine dissolution[17]

	Fouda et al (1996a)	Fouda et al (1996b)	Apostolidos and Distin (1978)	Teir et al (2006a)	Teir et al (2006b)	Teir et al (2006c)	Van Essendelft (2009)
Temperature	30-75°C (Roasted at 800°C for 2-3 h)	30-75°C (Roasted at 800°C for 2-3 h)	30-70°C (Roasted at 700°C for 6 h and 825°C for 2 h)	30-70°C	30-70°C	30-70°C	30-75°C
Acid	3M H_2SO_4	3M HNO_3	0.15-0.6M H_2SO_4	2M H_2SO_4	2M HCl	2M HNO_3	1M H_2SO_4
Activation Energy (kJ /mol)	35.6	72.8	50.2	68.1	70.4	74.3	60.0

The activation energy for the surface dissolution was briefly measured at a pH of 3.5 with and without acetate, which is the main product of anaerobic digestion of food waste. Determination of the activation energy requires the knowledge of reaction rates at two different temperatures. The effect of the reaction temperature on pH and activities of $acetate^-$ were simulated using Visual MINTQ. The pH differences at 25 °C and 50 °C for DI water and 0.01 M sodium acetate solution are insignificant. The activity difference for $acetate^-$ at 25 °C and 50 °C is only 1.2% for 0.01 M sodium acetate solution at pH 3.5.

Heating tape was used to pre-heat the solvents for the activity measurements. Because of the heat loss during the dissolution experiments, the real temperature of the solutions collected from the syringe pump reactor was only 45 °C while the desired set temperature was 50 °C. The real temperature measured by temperature sensor was used for the activation energy calculation. Figure 18 shows the initial dissolution rates with the first 5 data points under different temperatures with DI water at pH 3.5. For DI water, the dissolution rates can be written as:

$$r(mol/cm^2/s) = A a_{H^+}^{n_{H^+}} \exp(\frac{-E_a}{RT})$$

The ratio of two initial dissolution rates is same as the ratio of two slopes.

$$\frac{r_1}{r_2} = \frac{\exp(\frac{-E_a}{RT_1})}{\exp(\frac{-E_a}{RT_2})} = \frac{Slope_1}{Slope_2}$$

The activation energy is determined to be 14.24 kJ/mol, which is very low due to higher dissolution rates achieved as a result of disordered surfaces.

Figure 19 shows the initial dissolution rates with all the data points (should be 20 points in the 6 min, but by mistake the last point was missed) under different temperatures. The activation energy is calculated to be 31.65 kJ/mol, but with all the data points it was found that the conversion curves were not linear. Figure 20 shows the initial dissolution rates with last 8 data points under different temperatures. The activation energy is calculated to be 38.48 kJ/mol.

For the solvents 0.01 M sodium acetate, the dissolution rates can be written as:

$$r(mol/m^2/s) = A_1 a_{H^+}^{n_{H^+}} \exp(\frac{-E_{a_1}}{RT}) + A_2 a_{L^-}^{n_{L^-}} \exp(\frac{-E_{a_2}}{RT})$$

The first part in the equation is proton-promoted dissolution rate and the second part is the ligan-promoted dissolution rate. Assuming the activation energy of proton-promoted dissolution is same as the one calculated above, the activation energy of ligan-promoted dissolution can be calculated by the following equation:

$$\frac{r_{T_1,Wligand} - r_{T_1,W/Oligand}}{r_{T_2,Wligand} - r_{T_2,W/Oligand}} = \frac{\exp(\frac{-E_{a,ligand-promoted}}{RT_1})}{\exp(\frac{-E_{a,ligand-promoted}}{RT_2})}$$

Figure 21 shows the initial dissolution rates with the first 5 data points under different temperatures with 0.01 M sodium acetate at pH 3.5. The activation energy of acetate-promoted dissolution is calculated to be 22.31kJ/mol. Figure 22 shows the initial dissolution rates with all the data points (should be 20 points in the 6 min, but by mistake the last point was missed) under different temperatures with 0.01 M sodium acetate at pH 3.5 and the activation energy of acetate-promoted dissolution is calculated to be 51.90kJ/mol. Figure 23 shows the initial dissolution rates with last 8 data points under different temperatures with 0.01 M sodium acetate at pH 3.5 and the activation energy of acetate-promoted dissolution is calculated to be 56.49 kJ/mol.

Figures 18-20: Mineral dissolution rate estimations (pH 3.5, DI water)

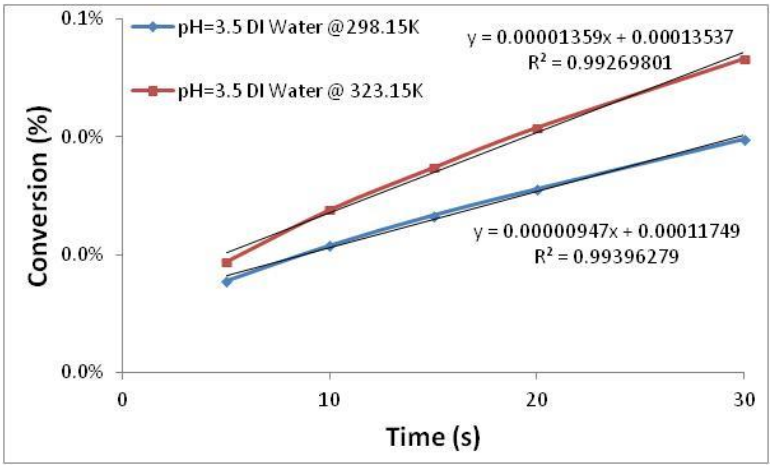

Figure18: Initial dissolution rates with first 5 data points under different temperatures

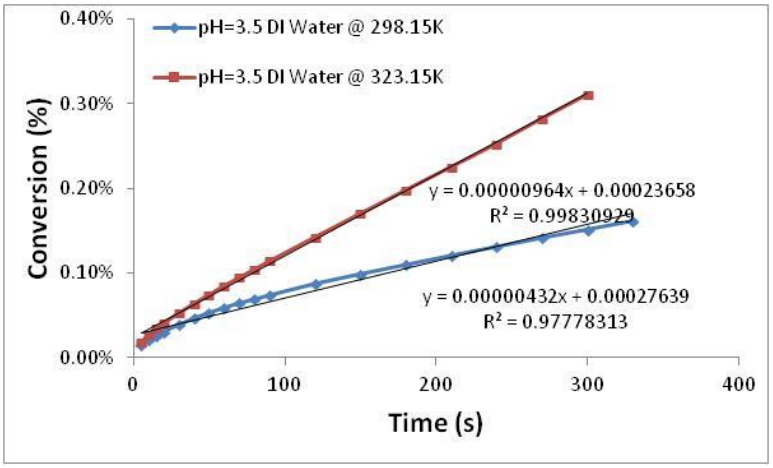

Figure 19: Initial dissolution rates with all the data points under different temperatures

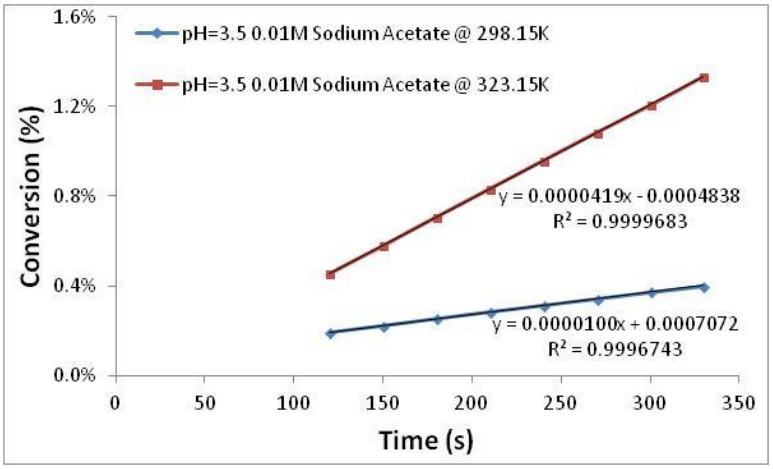

Figure 20: Initial dissolution rates with last 8 data points under different temperatures

Figures 21-23: Mineral dissolution rate estimations (pH 3.5, 0.01 M sodium acetate)

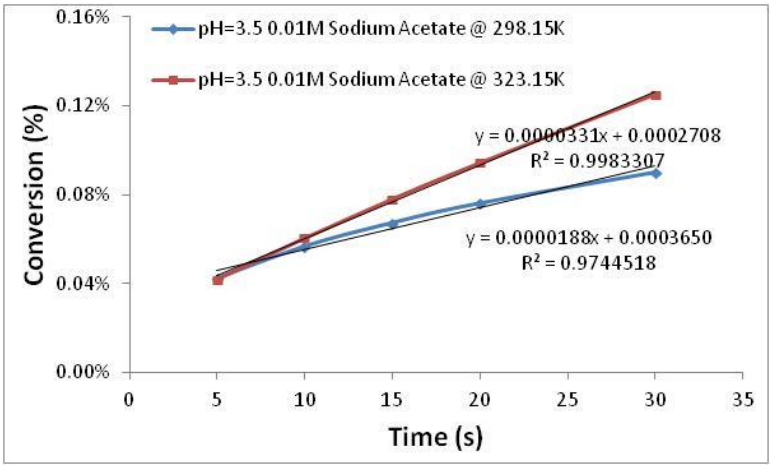

Figure 21: Initial dissolution rates with first 5 data points under different temperatures

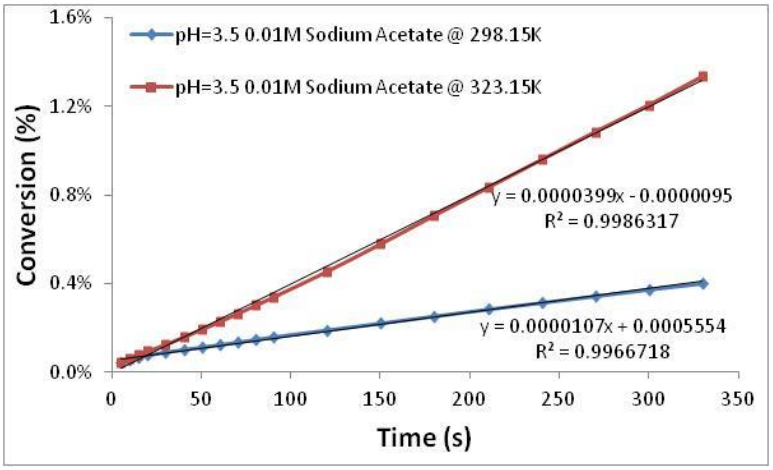

Figure 22: Initial dissolution rates with all the data points under different temperatures

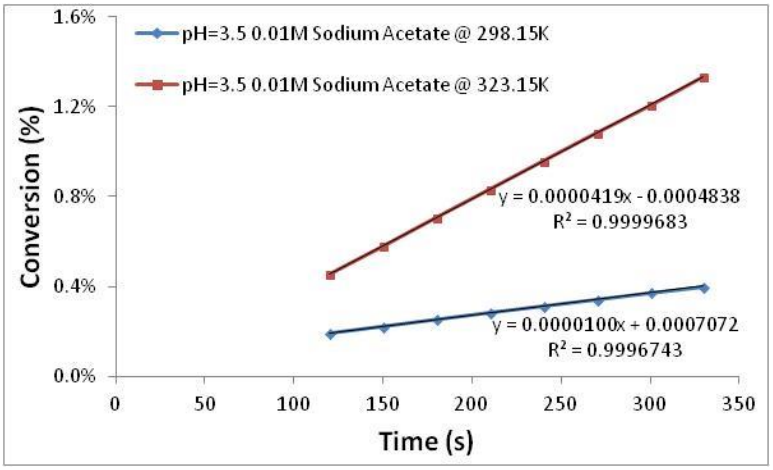

Figure 23: Initial dissolution rates with last 8 data points under different temperatures

5. Precipitated Magnesium Carbonates

PMC's application is broad including salt, cosmetics and toothpaste; however, its demand is rather limited. On the other hand, the demand for precipitated calcium carbonate (PCC) is strong in the paper, paints, and plastics/rubber industries. Since the PMC produced during the carbon mineral storage process is bright white pow(d?)er with high chemical and thermal stability, which are properties similar to PCC, new applications of PMC are proposed to replace PCC in various applications. This will not only provide an additional economic benefit to the carbon mineral storage process, but also lead to an avoidance of large quantities of CO_2 that is often emitted during the production of PCC.[20] In order to achieve this goal, PMC was synthesized with tailored properties such as the mean particle size, particle size distribution and surface morphology, to emulate some commercially made PCC particles.

In order to control and monitor the precipitation process while evaluating each experimental parameter, a batch system was used instead of a continuous system. A batch system is more likely to be used for large scale carbon mineral storage efforts.

First, the effect of aging time on PMC was studied at 295 K and 355 K. At 295 K, 150 mL of 0.5 M Na_2CO_3 solution and 150 mL of 0.5 M $Mg(NO_3)_2$ solution with 0.1 M sodium acetate were prepared for each run. These solutions were mixed in a glass reactor placed in a water bath to produce PMC. For all cases, the slurry was mixed at 800 rpm throughout experiment. 8 experiments with 8 different aging times (0.25 hour, 0.5 hour, 1 hour, 2 hours, 4 hours, 8 hours, 16 hours and 48 hours) were conducted for this study. At the end of each run, slurry samples were collected and the mean particle size and the particle size distribution were determined using a Beckman-Coulter LS 13320 Particle Sizer. Then slurry was filtered, and the filter cake was thoroughly washed with DI water and the solid products were dried with two methods – oven dry and freeze dry. Once dried, the solid samples were analyzed using a Scanning Electron Microscope (SEM) for their morphological structures. Thermogravimetric Analysis (TGA) and Raman spectroscopy were used for the analysis of chemical composition.

Figure 24 shows the effect of aging time on the mean particle size and particle morphological structure as well as the particle size distribution at 295 K. At short aging time, the mean particle size of PMC was around 15 micron and the particle size distrubution was broad, because PMC samples had need-like shape. For long aging time, the mean particle size of PMC was less than 10 micron and the particle size distrubution was narrow, due to phase change. Figure 3 and 4 show the evidence of phase chage. Theoretically, the weight loss of nesquehonite ($MgCO_3 \cdot 3H_2O$) is around 71 % during the calcination and the weight loss of hydromagnesite ($Mg_5(CO_3)_4(OH)_2 \cdot 4H_2O$) is around 57 %.

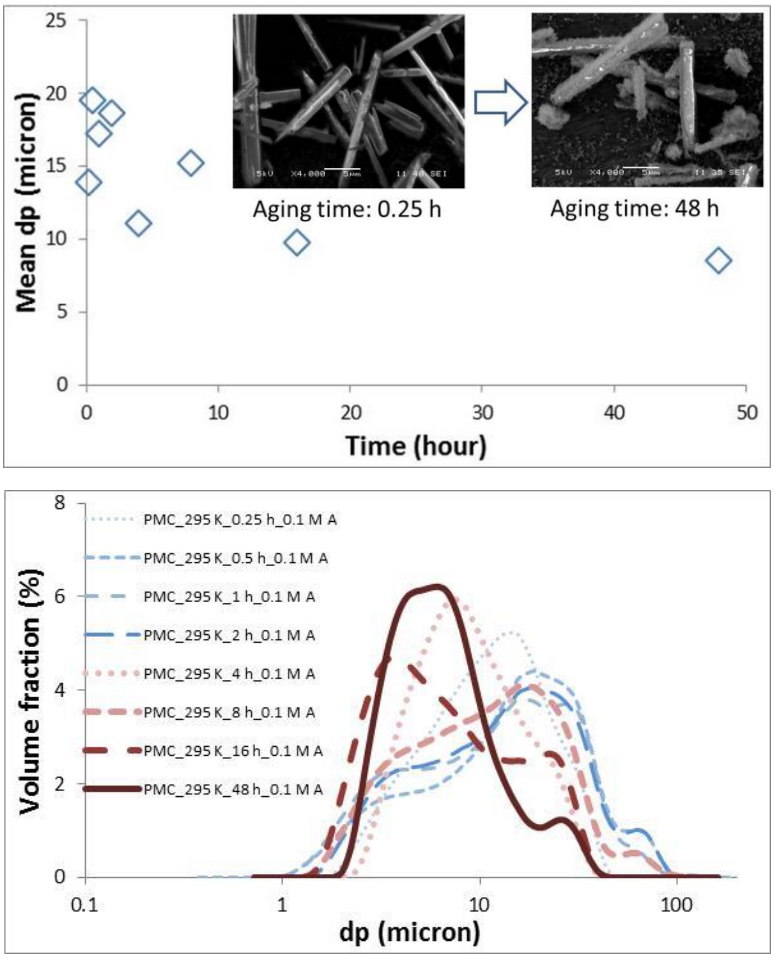

Figure 24: Effect of aging time on the mean particle size and particle morphological structure (top) as well as the particle size distribution (bottom) at 295 K

Figure 25 shows that for short aging time, the weight loss of PMC samples was around 70 %, and the samples should be nesquehonite with trace amount of hydromagnesite. But the weight loss of PMC sample, which had 48 hours aging time, was around 60 %. This reveals that the sample is a combination of nesquehonite and hydromagnesite which was also confirmed with SEM. There were some need-like (nesquehonite) and some small particles (hydromagnesite) in the PMC sample produced in 48 hours. Raman spectroscopy (Figure 26) shows a small peak around 3650 nm, which indicates the -OH group, for the PMC sample produced in 48 hours.

Figure 27 and Figure 28 show the effect of freeze drying vs. oven drying PMC samples. During the oven dry (overnight at 343 K), dehydration of nesquehonite occurred due to high temperature which resulted in converting nesquehonite samples to hydromagnesite. The differences between nesquehonite and hydromagnesite in Raman

spectroscopies are that nesquehonite has main peak at 1105 nm and hydromagnesite has main peak at 1130 nm as well as a peak at 3650 nm.

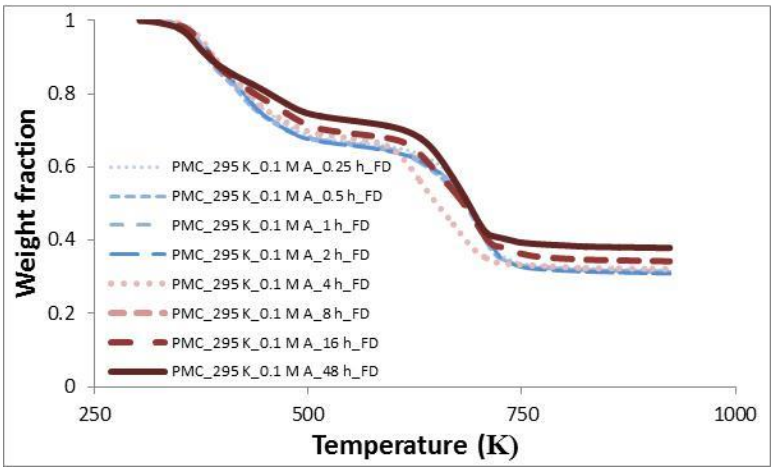

Figure 25: Effect of aging time on the thermal decomposition of PMC at 295 K

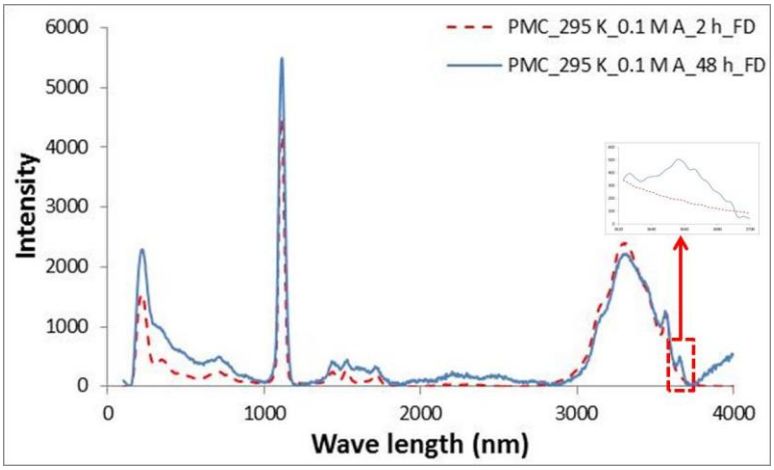

Figure 26: Effect of aging time on the chemical composition of PMC at 295 K

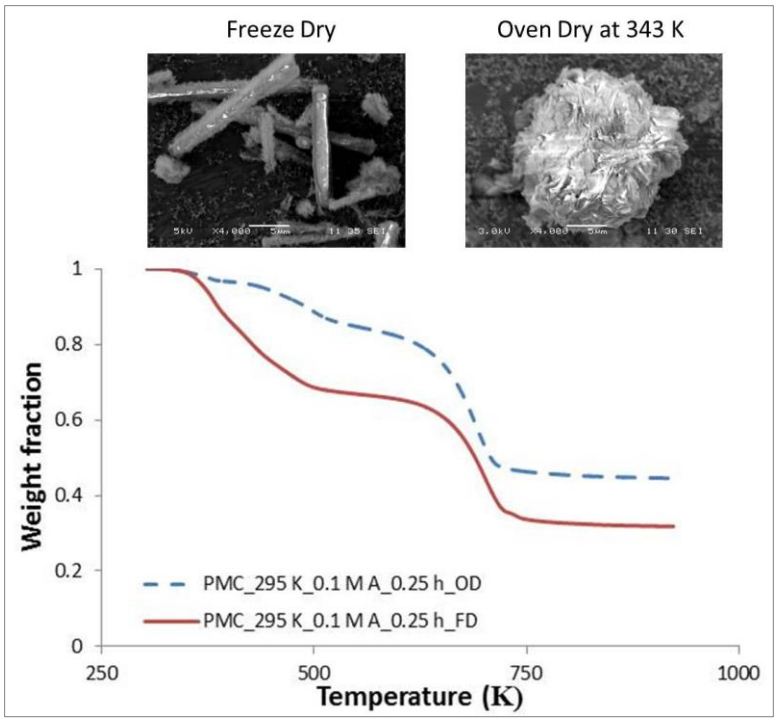

Figure 27: Effect of drying methods on the particle morphological structure and thermal decomposition of PMC

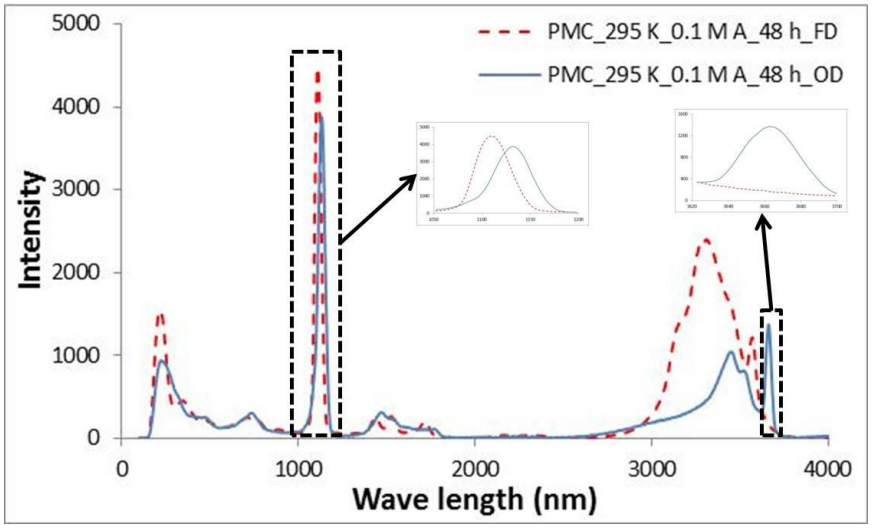

Figure 28: Effect of drying methods on the chemical composition of PMC

At 355 K, 150 mL of 0.5 M Na_2CO_3 solution and 150 mL of 0.5 M $Mg(NO_3)_2$ solution were prepared for each run. And experiments were conducted at 4 different aging times – 0.25 hour, 0.5 hour, 1 hour and 2 hours. The experimental process and characterization of PMC were same as the ones mentioned above. The only difference was all the slurry samples were dried with the Freeze Dryer alone.

At 355 K, the effect of aging time on PMC was not significant. Mean particle size decreased a little with longer aging time, but the particle size distributions were almost same as shown in Figure 29 Moreover, there was no difference between Raman spectroscopies as represented in Figure 30.

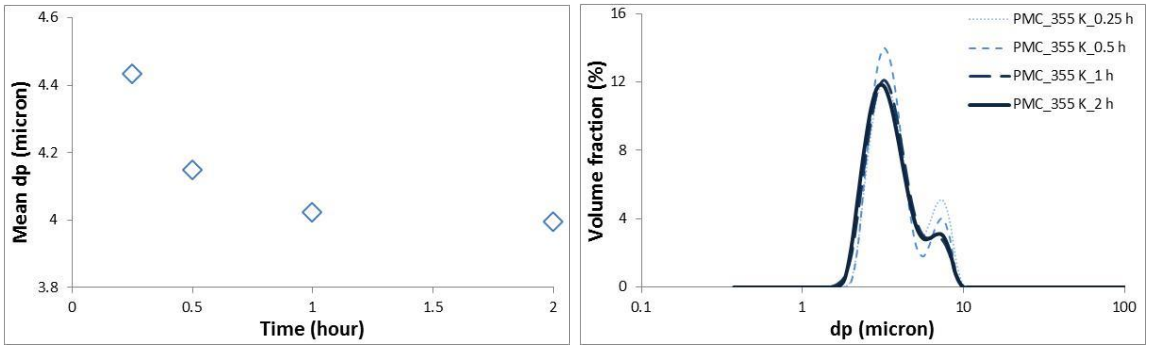

Figure 29: Effect of aging time on the mean particle size (top) and the particle size distribution (bottom) at 355 K

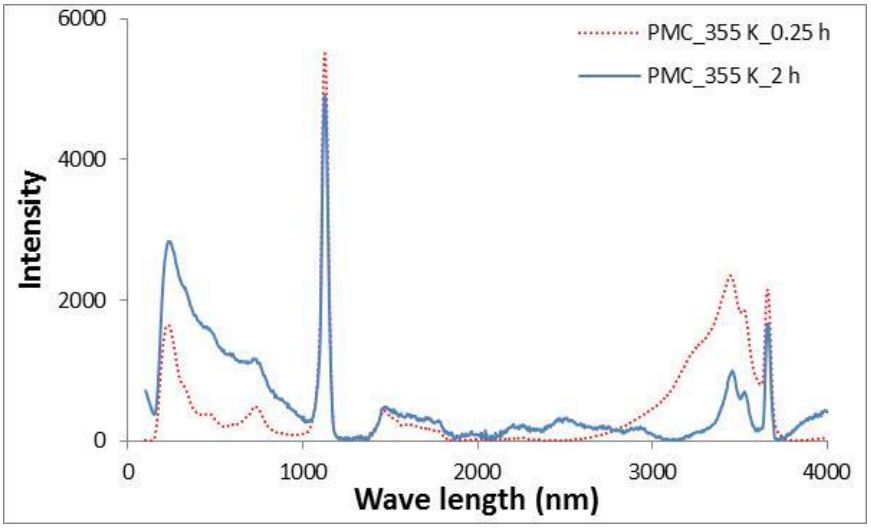

Figure 30: Effect of aging time on the chemical composition of PMC at 255 K

Second, the effect of reaction temperature on PMC was studied. For each experiment, 150 mL of 0.5 M Na_2CO_3 solution and 150 mL of 0.5 M $Mg(NO_3)_2$ solution with 0.1 M sodium acetate were prepared. Experiments were conducted at 4 different reaction temperatures – 295 K, 315 K, 335 K and 355 K. Aging time was 2 hours for each run. The experimental process and characterization of PMC were same as the ones mentioned above. The slurry samples were dried with the Freeze Dryer.

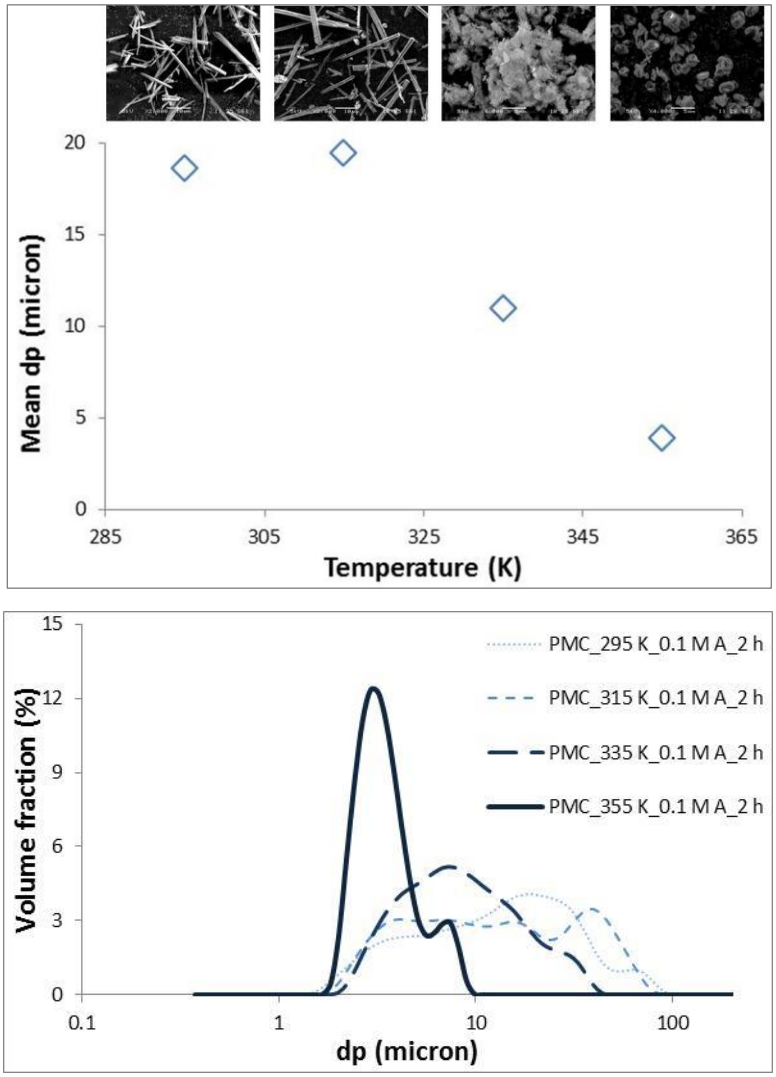

Figure 31: Effect of reaction temperature on the mean particle size and particle morphological structure (top) as well as the particle size distribution (bottom) (aging time: 2 hours)

Figure 31 shows that the effect of the reaction temperature on the particle size and the morphological structure were quite strong. As the reaction temperature increased from 295 K to 355 K, the particle shape changed from needle-like to rosette-like

crystallites and the mean particle size was reduced from 20 micron to 4 micron. The particle size distribution also became considerably narrower at higher reaction temperatures. Figure 32 and Figure 33 show that PMC samples produced at 295 K and 315 K were nesquehonite and PMC samples produced at 335 K and 355 K were hydromagnesite. Figure 32 shows that weight loss of PMC samples produced at 295 K and 315 K were around 70% and weight loss of PMC samples produced at 335 K and 355 K were around 55%.

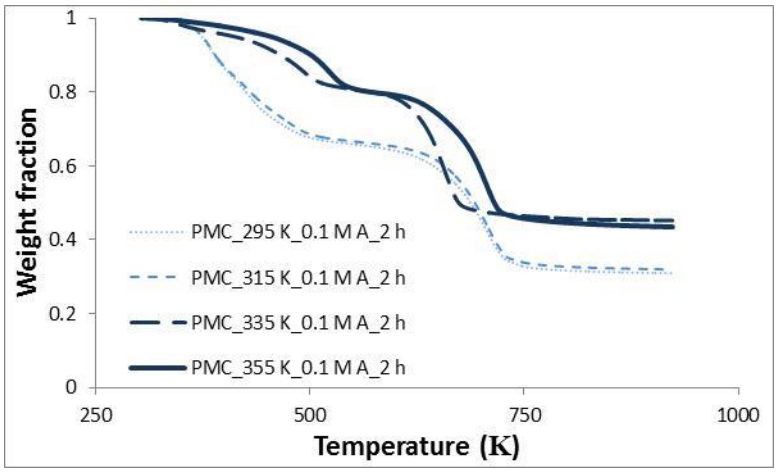

Figure 32: Effect of reaction temperature on the thermal decomposition of PMC (aging time: 2 hours)

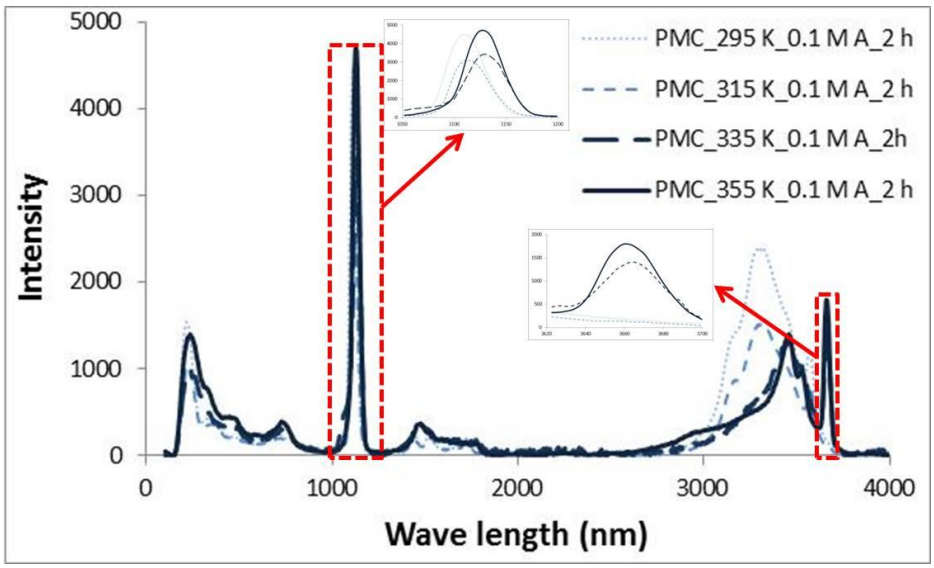

Figure 33: Effect of reaction temperature on the chemical composition of PMC (aging time: 2 hours)

Third, the effect of chelating agents on PMC was studied. Since acetate, propionate, succinate and valerate are the final products in the process of anaerobic digestion of food waste in the microbial reactor and acetate and propionate are the main products, three additives – acetate, propionate and mixture of 4 chelating agents were selected for this study. For each experiment, 150 mL of 0.5 M Na_2CO_3 solution and 150 mL of 0.5 M $Mg(NO_3)_2$ solution with or without different additives were prepared. The three different additives were 0.1 M sodium acetate, 0.1 M propionate and mixture (0.022 M sodium acetate, 0.015 M sodium propionate, 0.004 M sodium succinate and 0.002 M sodium valerate). Experiments were conducted at 2 different reaction temperatures – 335 K and 355 K, and the aging time was 2 hours for each experiment. The experimental process and characterization of PMC were same as the ones mentioned above. The slurry samples were dried with the Freeze Dryer.

Figure 34 shows that the effect of chelating agents on the mean particle size and the particle size distribution could be neglected at 335 K and 355 K. However, Figure 35 shows that chelating agents may affect the formation of PMC at 335 K. TGA results of 4 PMC samples (without chelating agent, with 0.1 M sodium acetate, with 0.1 m sodium propionate and with mixture of chelating agents), which were produced at 355 K, were exactly alike. For 4 PMC samples produced at 335 K, however, TGA results were different. The weight losses were similar, but the decomposition occurred at different temperatures. In the future, a Carbon Analyzer that can determine Total Carbon including Inorganic and Organic Carbon will be used to confirm the chemical composition of PMC samples. Raman spectroscopies as shown in Figure 36 represent the same phenomena. There were some differences among the PMC samples produced at 335 K with various chelating agents.

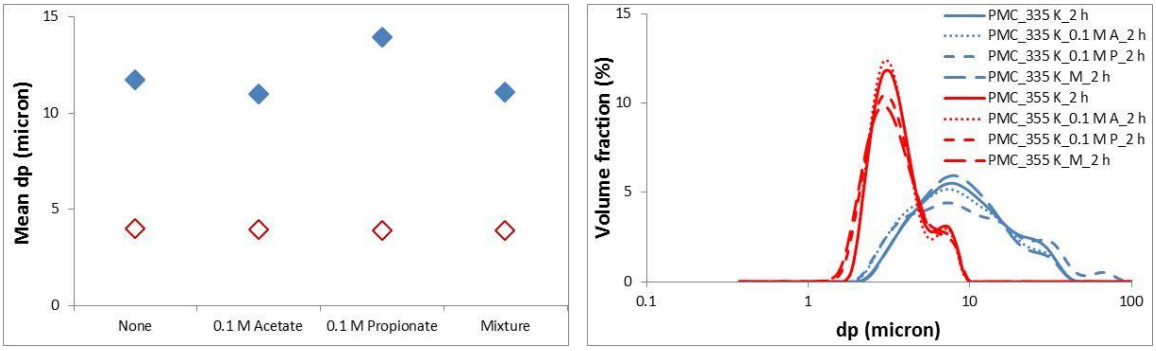

Figure 34: Effect of chelating agents on the mean particle size (top) and the particle size distribution (bottom) (Red: 355 K, Blue: 335 K) (aging time: 2 hours)

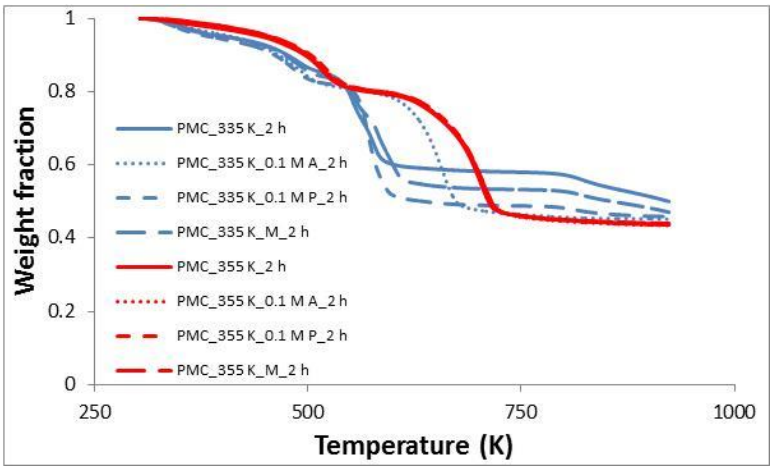

Figure 35: Effect of chelating agents on the thermal decomposition of PMC (aging time: 2 hours)

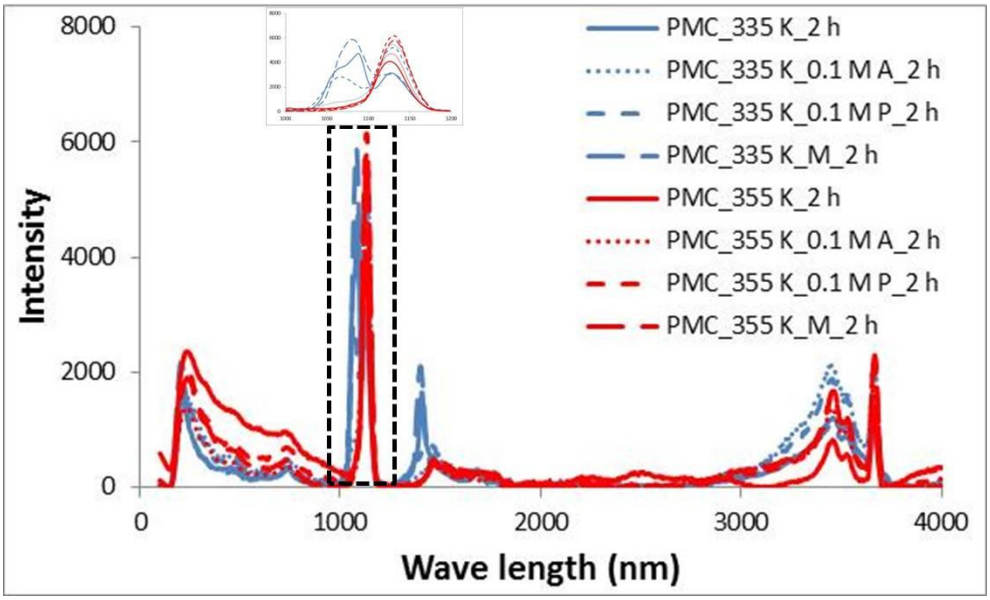

Figure 36: Effect of chelating agents on the chemical composition of PMC (aging time: 2 hours)

6. In-Situ Mineral Carbonation

A high temperature, high pressure batch reactor is used to mimic in-situ mineral carbonation. 7.5 mg of raw antigorite mineral, 42.5 ml of the prepared solvent (e.g. DI water, sodium oxalate etc.) and liquid CO_2 are fed into the batch reactor which is then pressurized to 75 bars by a syringe pump. The contents are mixed to allow for effective heat and mass transfer. First, the reactor was heated to the desired reaction temperature in 30 minutes, and then the pressure of system was increased from 75 bars to the desired level by a syringe pump and the timing began. Once the reaction was completed (reaction time: 2 hours or 4 hours), the reactor was cooled to around 60 °C in 70 minutes, depressurized and the contents were filtered. The extent of carbonation was determined using a TGA. Changes in particle and pore size distribution and surface morphology were also determined by SEM. In this part, effect of reaction temperature, partial pressure of CO_2, and reaction time were investigated. First, carbonation experiments were performed at three different temperatures (90 ºC, 120 ºC and 150 ºC) under a constant pressure of 90 atm. Second, carbonation experiments were performed under three different pressures (90 atm, 120 atm and 150 atm) at 150 ºC. Finally, carbonation experiments were performed with two different reaction times–2 hours and 4 hours, to study the effect of reaction time on mineral carbonation.

Figure 37 shows the effect of reaction temperature on single-step mineral carbonation. Partial pressure of CO_2 was fixed at 90 bars, and reaction time was 2 hours for each run. Solvent used for this study was mixture of weak organic acids from the microbial reactor. The conversion was increased from 9.24% to 11.33% when the reaction temperature was increased from 90 ºC to 150 ºC. Mineral dissolution favors high temperatures, while mineral carbonation favors low temperatures. Considering both kinetics and thermal, however, single-step mineral carbonation favors high temperature.

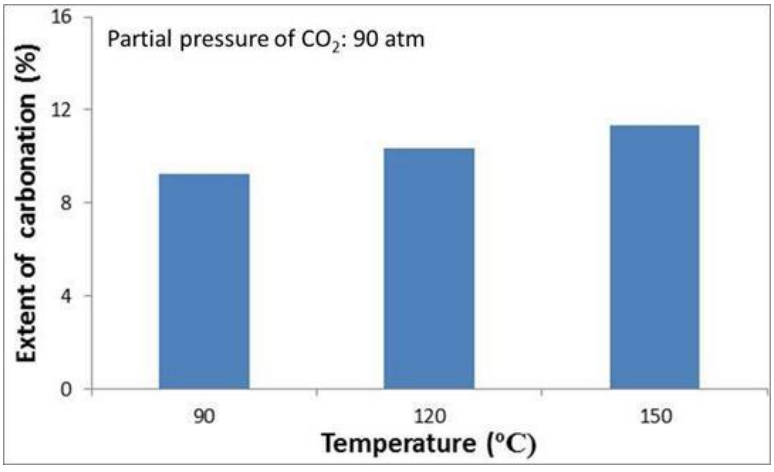

Figure 37: Effect of reaction temperature on single-step mineral carbonation

Figure 38 shows the effect of partial pressure of CO_2 on single-step mineral carbonation. Reaction temperature was fixed at 150 ºC, and reaction time was 2 hours for each run. Solvent used for this study was mixture of weak organic acids from the microbial reactor. When the partial pressure of CO_2 was 120 bars, the maximum conversion was achieved. Mineral dissolution favors low pH, while mineral carbonation favors high pH. It seems that under the partial pressure of CO_2 of 120 bars, the system pH was achieved the optimal condition.

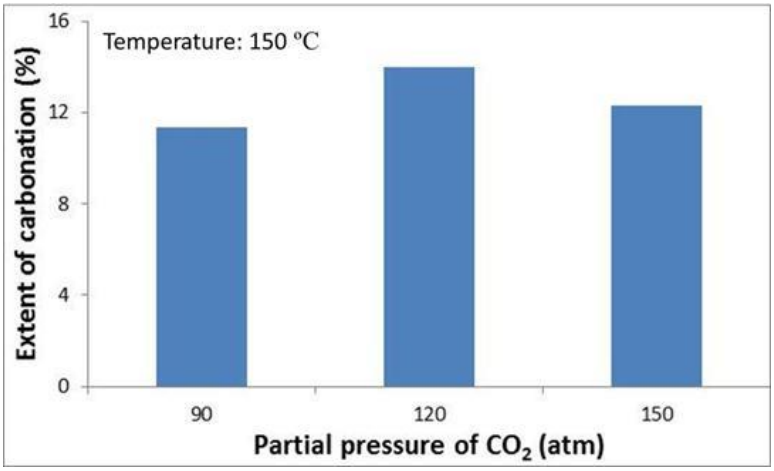

Figure 38: Effect of partial pressure of CO_2 on single-step mineral carbonation

The effect of reaction time on single-step mineral carbonation was investigated under the CO_2 pressure of 150 bars at 150 ºC with the solvent of the mixture of weak organic acids from the microbial reactor. As expected, the conversion was increased by around 2 %, while the reaction time was increased from 2 hours to 4 hours (Figure 39).

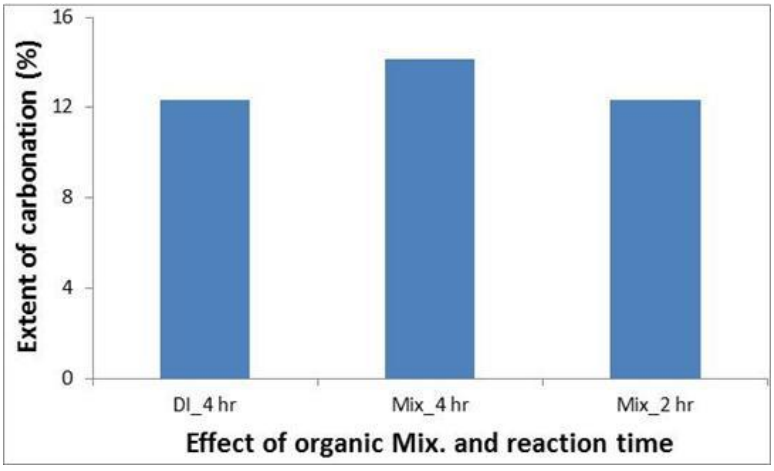

Figure 39: Effect of reaction time and organic mixture on single-step mineral carbonation

Figure 40 shows the effect of other chemical additives on the single-step mineral carbonation. Experiments were performed under the partial pressure of CO_2 of 120 bars at 150 ºC with various chemical additives. The reaction time was 2 hours for each run. Conversions were all around 12 %. Once the carbonation experiment was done, the contents were filtered and the solution composition was analyzed by ICP-OES. It was found that total magnesium concentration in the solution was only several hundred ppm, and the final pH of the solution was around 7.5 for each experiment. It seems that the fine particles in the raw antigorite minerals were dissolved and carbonated fast, but the dissolution of large particles was very slow for some reasons. High pH of the solution in the reactor was one possible reason, and another one is the formation of the passivation layers for the large particles which are the barriers for the diffusion. SEM photos (Figure 41) also show that there was no clear crystallized magnesite on the surface of the large particles.

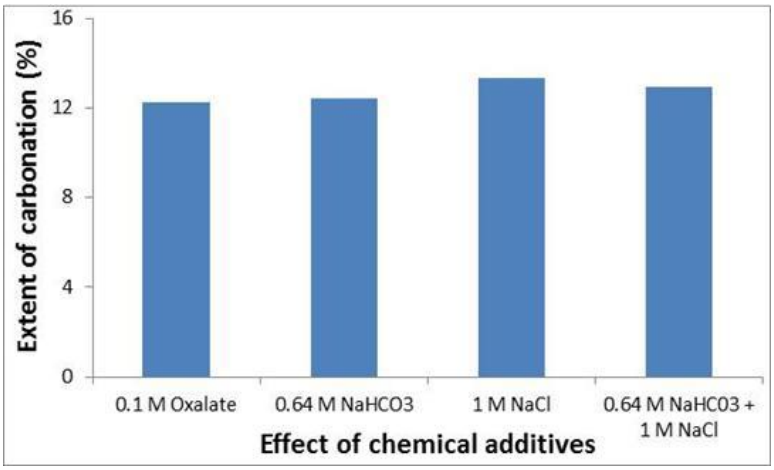

Figure 40: Effect of various chemical additives on single-step mineral carbonation

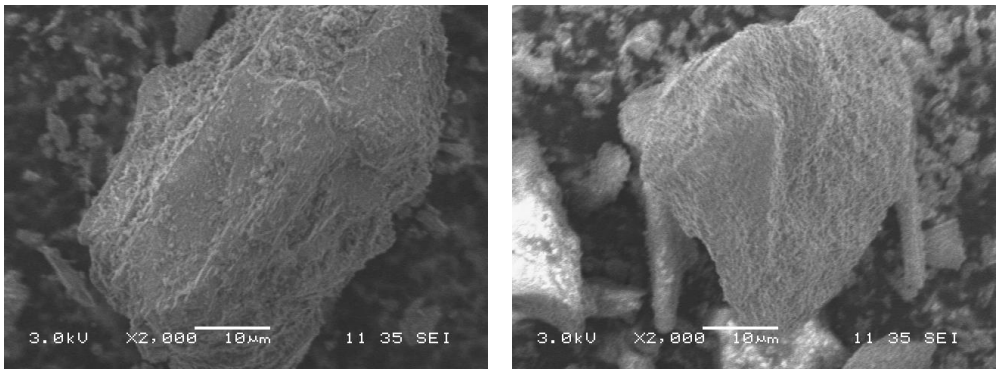

Figure 41: SEM images of the large antigorite particles after single-step mineral carbontion

To compare with the results of olivine carbonation (DOE Award Number: DE-FE0002386), the team changed experiment conditions and studied the effects of reaction temperature, pressure, reaction time and various chemical additives on antigorite carbonation again. Carbonation experiments were performed at four different temperatures (90 ºC, 125 ºC, 150 ºC and 185 ºC) under a constant CO_2 partial pressure of 150 atm. Carbonation experiments were also performed under four different pressures (75 atm, 100 atm 150 atm and 175 atm) at 185 ºC. Reaction time was 3 hours for each experiment and salt solvent (1.0M NaCl+0.64M $NaHCO_3$) was used to enhance the rate of mineral carbonation. The effect of reaction time on antigorite carbonation was studied also. Finally, the effect of various chemical additives on antigorite carbonation was investigated. Sodium bicarbonate, sodium chloride and the mixture of sodium bicarbonate and sodium chloride were used to enhance the reaction rate of mineral carbonation.

Figure 42 shows the effect of reaction temperature on single-step mineral carbonation. Partial pressure of CO_2 was fixed at 150 atm, and reaction time was 3 hours for each experiment. Solvent used for this study was a mixture of 0.64 M $NaHCO_3$ and 1 M NaCl. The conversion was increased from 10.74% to 14.07% when the reaction temperature was increased from 90 ºC to 185 ºC. In olivine carbonation, however, a substantial increase in mineral carbonation was observed with increasing temperature (from 1.84 % to 71.09 %). Mineral dissolution favors high temperature, while mineral carbonation favors low temperature. Considering both kinetics and thermodynamic, single-step mineral carbonation favors high temperature.

The effect of partial pressure of CO_2 on single-step mineral carbonation is illustrated in Figure 43. Reaction temperature was fixed at 185 ºC, and reaction time was 3 hours for each experiment. Solvent used for this study was a mixture of 0.64 M $NaHCO_3$ and 1 M NaCl. When the partial pressure of CO_2 was 150 atm, the maximum conversion was achieved. Mineral dissolution favors low pH, while mineral carbonation favors high pH. It seems that under the partial pressure of CO_2 of 150 atm, the system pH that was achieved was the optimal condition. In olivine carbonation, the maximum conversion was achieved at the partial pressure of CO_2 was 150 atm also, but a substantial increase in mineral carbonation was observed with increasing partial pressure of CO_2 from 75 atm to 150 atm (around 40% increase in conversion).

The reaction time on single-step mineral carbonation resulted in similar trend. Experiments were performed at 150 ºC under a partial pressure of CO_2 of 150 atm. Solvent used for this study was mixture of 0.64 M $NaHCO_3$ and 1 M NaCl. As expected, the conversion was increased by around 2.5%, while the reaction time was increased from 1 hour to 5 hours. It seems that most antigorite carbonation occurred during the first one hour. In olivine carbonation, however, after the first one hour, an additional 30% carbonation was observed when the reaction time was 5 hours (Figure 44).

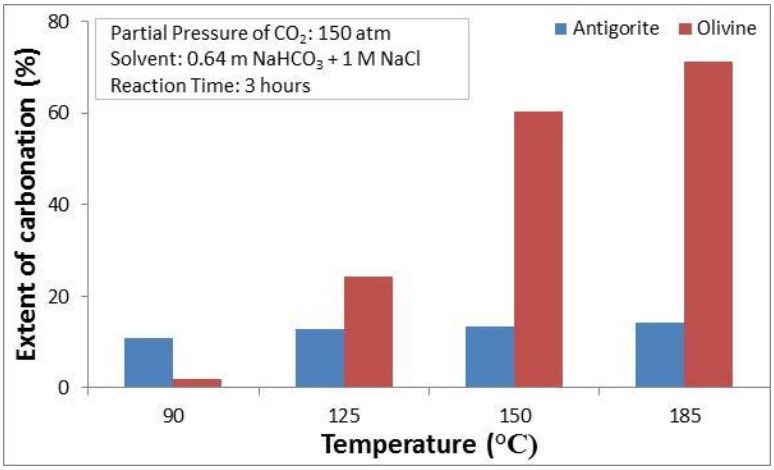

Figure 42: Effect of reaction T on single-step antigorite and olivine carbonation

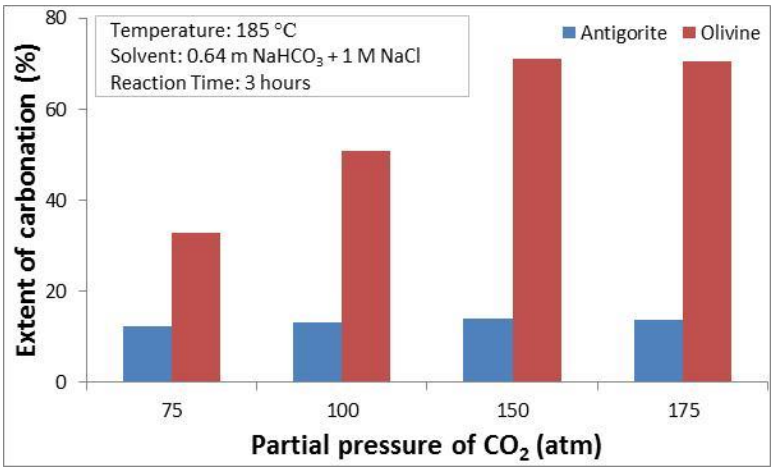

Figure 43: Effect of P_{CO2} on single-step antigorite and olivine carbonation

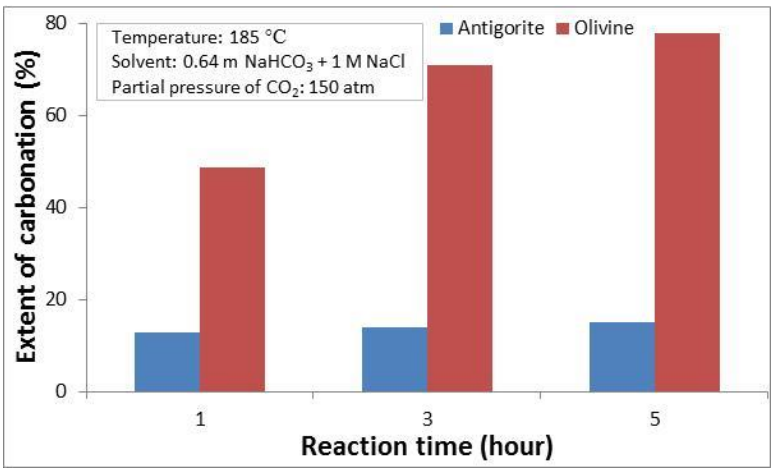

Figure 44: Effect of reaction time on single-step antigorite and olivine carbonation

Figure 45 shows the effect of various chemical additives on the single-step mineral carbonation. Experiments were performed under a partial pressure of CO_2 of 150 atm at 185 ºC with various chemical additives. The reaction time was 3 hours for each experiment. For antigorite minerals, conversions were all around 14%. However in olivine carbonation, the chemical additives worked very well. There was a significant increase in extent of carbonation with 0.64 M $NaHCO_3$, 1 M NaCl and the mixture of 0.64 M $NaHCO_3$ and 1 M NaCl.

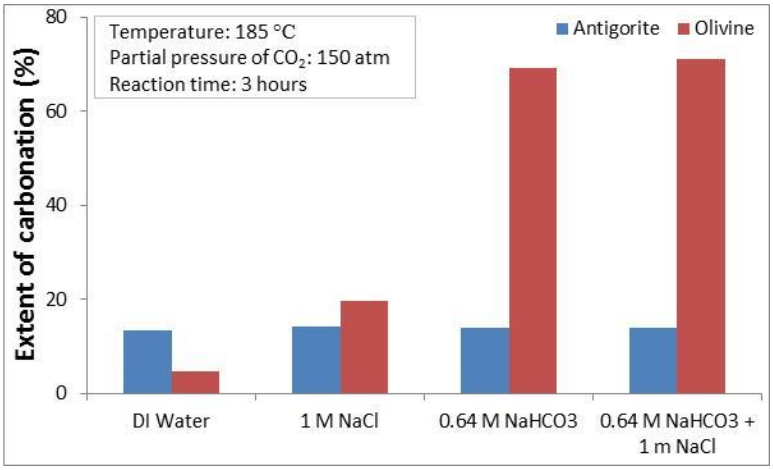

Figure 45: Effect of various chemical additives on single-step antigorite and olivine carbonation

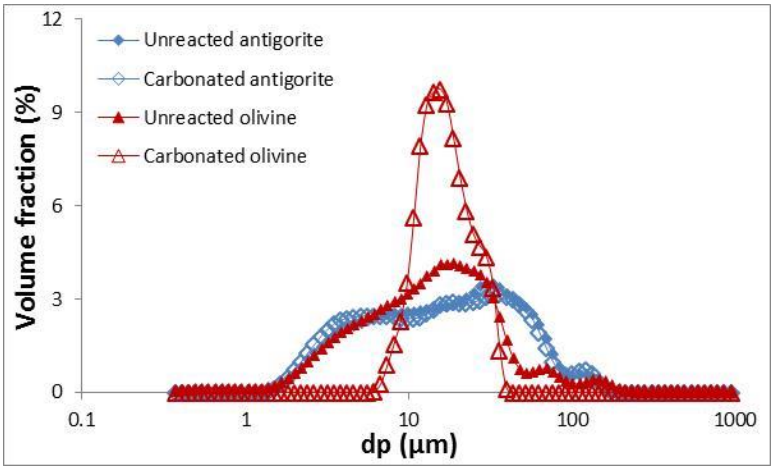

Figure 46: Particle size distrubution of unreacted antigorite and carbonated antigorite

Particle size distribution (Figure 46) shows that there was no difference between unreacted antigorite minerals and carbonated antigorite minerals. It seems that only fine particles were carbonated in the reactor and the rate of mineral carbonation of large particles was very slow. Unlike olivine where more than 95% of the particles were smaller than 37µm, only about 80% of the antigorite sample was smaller than 37µm. One

of the reasons for the lower extents of carbonation observed with antigorite as opposed to olivine is attributed to the mass transfer limitation due to larger particles in the antigorite sample. Another reason for the lower extent of antigorite carbonation is its crystal structure which is more complex due to the presence of –OH groups. Antigorite mineral's old inert surface maybe affect antigorite carbonation also. Table 9 shows the effect of inert surface on olivine carbonation.

Table 9: Effect of inert surface on olivine carbonation

Olivine Sample Type	Freshly ground olivine sample	Old olivine sample
Reaction Conditions	1 M NaCl + 0.64 M NaHCO3, 185C, 150 atm, 3 hours	1 M NaCl + 0.64 M $NaHCO_3$, 185C, 150 atm, 3 hours
Particle Size Distribution	0.3-92 µm (95% < 37 µm)	10 – 90 µm
Extent of Carbonation	71.09%	1-2%

Antigorite minerals were reground and the one-step mineral carbonation experiment was repeated with reground minerals in high temperature and a high pressure reactor. However, there was no big difference between the carbonation of old antigorite minerals and reground antigorite minerals (Figure 47).

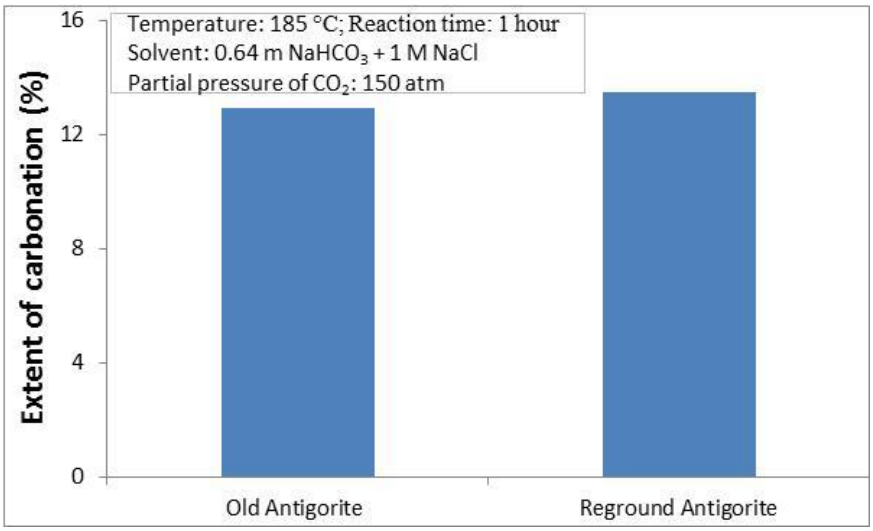

Figure 47: Comparison of mineral carbonation with old antigorite particles and mineral carbonation with reground antigorite particles

7. Environmental Risk Analysis of Chemically Enhanced In-Situ Mineral Carbonation via Volatile Fatty Acid

Our proposed chemically enhanced in-situ mineral carbonation via volatile fatty acids which were produced by the process of anaerobic digestion of food waste was compared with the normally in-situ mineral carbonation and sanitary landfills. Several possible additional environmental issues, which may be caused by the injection of the volatile fatty acids into the underground, were also discussed. Since my colleagues are working on the risk analysis of in-situ mineral carbonation, in this report only the issues which were related to the injection of volatile fatty acids into the underground were discussed.

(a) CH_4 formation

Injected volatile fatty acids may be decomposed by some bacteria underground (anaerobic digestion) and make CH_4 gas, which traps 23 times more heat than carbon dioxide will over the next 100 years.[21] However, considering the high temperature (over 90 °C) condition, this anaerobic digestion caused by the bacteria, as in the process of landfills, would probably not happen. If continued anaerobic digestion happened and made some CH_4 gas, CH_4 gas still can be sequestrated with carbon dioxide underground, because the injection sites are isolated systems. In that case, additional volatile fatty acids, which are considered to work as catalysts for mineral carbonation, should be injected into the underground based on the rate of anaerobic digestion.

(b) Heavy metals release

In landfills, accumulation of heavy metals is an environmental issue. The heavy metals are from the municipal solid wastes.[22] In this particular project, volatile fatty acids produced by the process of anaerobic digestion of food waste will be injected into the underground. These acids don't contain any heavy metals, but they can enhance the dissolution of silicate minerals, which usually contain some level of heavy metals, and release heavy metals. Considering the injection site as an isolated system, if there is no water exchange between the injection site and groundwater, accumulation of leached out heavy metals may not be a problem. Dissolved heavy metals (metal-ligand complexes) should go with the water flow.

(c) Contamination of ground water

Contamination of ground water is an issue of in-situ mineral carbonation. However, most of injection sites are very deep (over 1000 m) and saline formation is preferred for in-situ mineral carbonation. Drinking water is usually taken from 100 m depth at most.[23] Compared to highly concentrated carbon dioxide, injected volatile fatty acids are not a

major contaminant for groundwater, if the isolated system was broken by some reason and caused water exchange. However, in this case dissolved heavy metals should be the main contaminant. Carbon dioxide may cause a huge pH change in ground water as well. Volatile fatty acids, however, may be decomposed by a process of anaerobic digestion if they escape from the injection sites.

(d) Enhanced dissolution of silicate minerals

Injected volatile fatty acids may cause the enhanced dissolution of silicate minerals as we proposed. This enhanced mineral dissolution may cause a little bigger change in porosity, permeability and volume than normal in-situ mineral carbonation. Figure 48 (DE-FE0002386) shows the porosity changes during the in-situ mineral carbonation. Enhanced mineral dissolution by injected volatile fatty acids will cause the acceleration of mineral carbonation. Mineral carbonation may cause porosity decrease or cracking of the rocks. If the porosity of rock decreases with carbonation, it is safe for carbon dioxide storage as mechanical strength increases. If there is rock cracking happening, the situation is a little more complicated. Poor caprock seal may cause some problems, because it may cause changes in geological formations. However, considering the slow kinetics of in-situ mineral carbonation, which may take years to weather the silicate minerals, it is possible to handle the changes with careful monitoring.

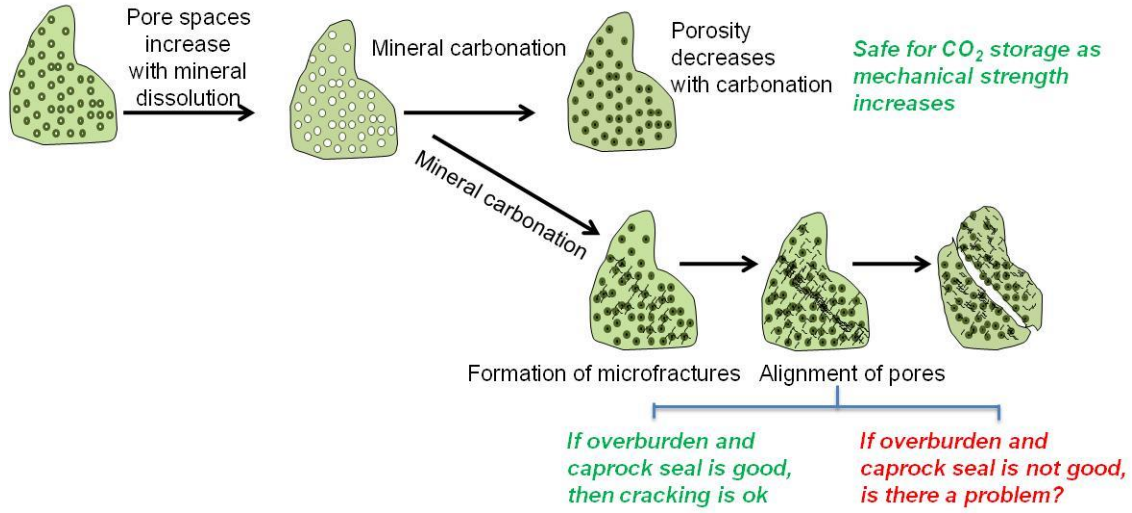

Figure 48: Changes of porosity of rock in in-situ mineral carbonation

8. Estimated Costs of Production of the Volatile Fatty Acids

Since our study is only lab-scale, we don't have our own data to estimate the costs of production of volatile fatty acids in industry-scale. The calculation of costs of production of the volatile fatty acids presented in this report is mainly based on several published studies of the anaerobic digestion system.

The main costs of anaerobic digestion include installation and operating costs. The necessary equipment to produce bioenergy from food wastes includes equipment to weigh and receive feedstock, feedstock preprocessing equipment, storage of feedstock prior to digestion, digester, energy generation equipment, and hydrogen sulfide clean-up equipment.[24] The costs of energy generation equipment, which is an unnecessary part of this study, are 36% of the total costs.[21] In this study, tipping fees for food waste (the money for the disposal of the food waste), which should be lower than landfills what charge, can be an income.[21] There are no heat sales and electricity sales, since our goal is to produce the volatile fatty acids which are known as intermediate products of the anaerobic digestion process.

(a) Cost of methane production

Approximate costs of production of biogas, which contains approximately 50-65% methane and 50-35% carbon dioxide[21], were calculated based on the following data.

Table 10: Financial & Technical Parameters of an Anaerobic Digestion System Utilizing Food Waste as Feedstock without Energy Generation Equipment[12]

Capital Cost	$360/ton food waste
Operation & Maintain Cost	$48/ton food waste
Tipping Fee	$20/ton food waste
Interest Rate & Debt Payment	7% & 15 years
Volatile Solids (VS)	531 lbs/ton food waste
Biogas Production Rate	15 ft^3 biogas/lb VS
Methane to Biogas Ratio	0.6
Captive Energy to Operate The Plant	10% produced biogas

For our system, to calculate the costs of methane production, we made several assumptions:

- We are using a model similar to the low scenario anaerobic digestion system and feedstock proposed in Kristi Moriarty study.[24] However, our system will not contain energy generation equipment, so the capital cost is $360 per ton of food waste which is 64% of $561 per ton of food waste (the average cost for a new average size digester).[24]
- Although our system will not contain energy generation equipment, we assume that captive energy necessary to operate the plant is equal to the energy released by the combustion of 10% produced biogas.

First, the excess biogas (10% produced biogas used as energy source for operating the anaerobic digestion system) produced by the system was calculated.

$$Excess\ produced\ biogas$$

$$= 531 \frac{lbs\ VS}{ton\ food\ waste} \times 15\ \frac{ft^3\ biogas}{lb\ VS} \times (1 - 0.1) = 7168.5\ \frac{ft^3\ biogas}{ton\ food\ waste}$$

Capital cost is $360 per ton of food waste, and this money will be paid in 15 years with 7% interest. Operation and maintain cost is $48 per ton of food waste, and the tipping fee is $20 per ton of food waste. Tipping fees for food waste must be lower to incentivize separation of wastes and collection and delivery by private waste haulers (landfills charge $30 per ton of food waste).[24]

$$Annual\ cost\ of\ anaerobic\ system$$

$$= \frac{\$360}{ton\ food\ waste} \times \frac{0.07}{1 - (1 + 0.07)^{-15}} + \frac{\$48}{ton\ food\ waste} - \frac{\$20}{ton\ food\ waste}$$

$$= \frac{\$67.53}{ton\ food\ waste}$$

$$Cost\ of\ production\ of\ biogas$$

$$= \frac{\$67.53}{ton\ food\ waste} \div 7168.5\ \frac{ft^3\ biogas}{ton\ food\ waste} = 0.942 \frac{cent}{ft^3\ biogas}$$

Since 60% of produced biogas is methane, the cost of methane production via anaerobic digestion of food waste is:

$$Cost\ of\ production\ of\ methane$$

$$= 0.942 \frac{cent}{ft^3 biogas} \div 0.6\ methane/biogas = 1.57 \frac{cent}{ft^3\ methane} = \frac{\$1.57}{therm\ methane}$$

One British therm is a non-SI unit of heat energy equal to 100,000 British thermal units (BTU). It is approximately the energy equivalent of burning 100 cubic feet of natural gas.

The average commercial cost for natural gas from 1996 to 2006 is 1.13 dollar per therm,[21] which is approximately 72% of the cost of production of methane via anaerobic digestion of food waste.

$$Carbon\ dioxide\ emission\ of\ anaerobic\ digestion\ system\ per\ ton\ of\ food\ waste$$

$$= 7168.5\ \frac{ft^3\ biogas}{ton\ food\ waste} \times 0.4\ \frac{CO_2}{biogas} +$$

$$531\ \frac{lbs\ VS}{ton\ food\ waste} \times 15\ \frac{ft^3\ biogas}{lb\ VS} \times 0.1$$

$$= 3663.9\ \frac{ft^3\ CO_2}{ton\ food\ waste}$$

$$= 3663.9\ \frac{ft^3\ CO_2}{ton\ food\ waste} \times \frac{28.3168\ L}{1\ ft^3} \div \frac{22.4\ L}{mol}$$

$$= 4.63\ \frac{kmol\ CO_2}{ton\ food\ waste}$$

$$CO_2\ emission\ of\ production\ of\ 1\ mol\ CH_4\ via\ anaerobic\ digestion\ of\ food\ waste$$

$$= 3663.9\ \frac{ft^3\ CO_2}{ton\ food\ waste} \div \left(7168.5\ \frac{ft^3\ biogas}{ton\ food\ waste} \times 0.6\ \frac{CH_4}{Biogas}\right)$$

$$= 0.85\ mol\ CO_2/mol\ CH_4$$

(b) Cost of acetate production

The cost of production of volatile fatty acids via anaerobic digestion of food waste was estimated. Volatile fatty acids are the intermediate products of anaerobic digestion

process, and usually anaerobic digestion is not an option for producing of volatile fatty acids. For example, most acetic acid is produced by methanol carbonylation. We did a theoretical calculation of costs of volatile fatty acids mixture production based on several assumptions in this report.

- Theoretically 70% of the carbon in methane is from acetate acetotrophic and 30% of carbon in methane is from hydrogen hydrogenotrophic.[14] However, reaction conditions can be changed to prevent the acetate acetotrophic and hydrogen hydrogenotrophic to form methane.
- All the volatile fatty acids are in the form of acetic acid by controlling the reaction condition.
- Capital cost, operation &maintain cost and tipping fee don't change.

First assumption is possible, but it's difficult to match the second assumption. However, usually acetic acid is the main inter intermediate product during the anaerobic digestion process, and it is possible to get concentrated acetic acid (more than 50% of volatile fatty acids in the form of acetic acid). In our previous experiments, acetic acid performed very well in antigorite dissolution.

$$Carbon\ which\ can\ be\ converted\ to\ CH_4\ in\ acetic\ acid$$

$$= 7168.5\ \frac{ft^3\ biogas}{ton\ food\ waste} \times \frac{28.3168\ L}{1\ ft^3} \div \frac{22.4\ L}{mol} \times 0.6\ \frac{CH_4}{biogas} \times 0.7$$

$$= 3806.0\ mol\ C/ton\ food\ waste$$

$$Mass\ of\ acetic\ acid\ from\ anaerobic\ digestion\ of\ food\ waste$$

$$= 3806.0\ \frac{mol\ C}{ton\ food\ waste} \div 2\ \times 60.05\ \frac{g}{mol} \div 1000\ \frac{g}{kg} \div 1000\ \frac{kg}{ton}$$

$$= 0.114\ ton\ acetic\ acid/ton\ food\ waste$$

$$Cost\ of\ production\ of\ acetic\ acid\ via\ anaerobic\ digestion\ of\ food\ waste$$

$$= \frac{\$67.53}{ton\ food\ waste} \div 0.114\ ton\ acetic\ acid/ton\ food\ waste$$

$$= \$592.4\ dollar/ton\ acetic\ acid$$

$$CO_2\ emission\ of\ production\ of\ 1\ mol\ acetic\ acid\ via\ anaerobic\ digestion\ of\ food\ waste$$

$$= \frac{Carbon\ in\ CO_2}{Carbon\ in\ acetic\ acid/2} = \frac{Total\ carbon - Carbon\ in\ acetic\ acid/2}{Carbon\ in\ acetic\ acid/2}$$

$$= \frac{531\frac{lbs\ VS}{ton\ food\ waste} \times 15\ \frac{ft^3\ biogas}{lb\ VS} - 7168.5\ \frac{ft^3\ biogas}{ton\ food\ waste} \times 0.7\ \div 2}{7168.5\ \frac{ft^3\ biogas}{ton\ food\ waste} \times 0.7\ \div 2}$$

$$= 2.17\ mol\ CO_2/mol\ acetic\ acid$$

The US marketing price of acetic acid is around $575 - 665 per ton of acetic acid.[25] The cost of production of acetic acid via anaerobic digestion of food waste is $592.4 per ton of acetic acid with low scenario anaerobic digestion system. It is a little cheaper than the average US marketing price of acetic acid ($620 per ton of acetic acid). However, the cost of methane production via anaerobic digestion of food waste is almost 1.5 times that of the commercial cost of methane production. It seems that production of volatile fatty acids via anaerobic digestion of food waste is economically feasible. If we can only prevent the acetate acetotrophic and keep hydrogen hydrogenotrophic to produce methane by controlling the reaction conditions, e.g. temperature, pH, the cost of acetic acid production will decrease due to the production of another valuable product (methane).

Considering the concentration of the volatile fatty acids as intermediate products of anaerobic digestion system (more than 0.2 M total VFAs)[26] and the COD level of volatile fatty acids in the young landfills, which can be more than 10000 (more than 0.1 M of total VFAs), it is possible and safe to inject 0.1 M total volatile fatty acids (this is the concentration of total VFAs in the pores underground) into geological formations with carbon dioxide. The mass of the acids depends on the total pore volume of the geological formation. Once the volatile fatty acids are injected, there should be no massive consumption of acids. We believe volatile fatty acids can work as catalysts. In mineral dissolution, they make magnesium-ligand complex or magnesium-proton-ligand complex, and during carbonation these complexes can react with carbonate to make carbonate minerals and release the ligands.

Additional injection of volatile fatty acids may be needed for some situations.

- Some bacteria may live under high temperatures (higher than 90 °C) and continue anaerobic digestion. This is a very unlikely case. However, considering the slow

decomposition of volatile fatty acids in landfills, the consumption should be very slow.

- Ligands may make some complexes with other metals than magnesium or calcium, for example heavy metals which are difficult to carbonate. We are looking for the effect of volatile fatty acids on heavy metal leaching and possible consumption by planning long term experiments or running the reactor at extreme conditions.
- Volatile fatty acids may be vaporized and escape from aqueous solutions. Volatile fatty acids have relatively low boiling points (120 – 200 ºC), and the temperature is over 90 ºC underground. The temperature depends on the depth of injection site.
- Since volatile fatty acids, e.g. acetic acid,[27] are thermally stable it is not possible for them to decompose because of the high temperature underground.

References

1. IPCC, *Carbon Dioxide Capture and Storage*. Cambridge University Press: Cambridge, 2005.
2. Baxter, P. J.; Kapila, M.; Mfonfu, D., "Lake Nyos disaster, Cameroon, 1986: the medical effects of large scale emission of carbon dioxide?" *British Medical Journal* 1989, 298, 1441-1444.
3. Lackner, K. S.; Wendt, C. H.; Butt, D. P.; Joyce, E. L.; Sharp, D. H., "Carbon Dioxide Disposal in Carbonate Minerals." *Energy* 1995, 20, (11), 1153-1170.
4. Goff, F.; Guthrie, G.; Lipin, B.; Fite, M.; Chipera, S.; Counce, D.; Kluk, E.; Ziock, H. *Evaluation of Ultramafic Deposits in the Eastern United States and Puerto Rico as Sources of Magnesium for Carbon Dioxide Sequestration*; 2000.
5. O'Connor, W. K.; Dahlin, D. C.; Nilsen, D. N.; Gerdemann, S. J.; Rush, G. E.; Penner, L. R.; Walters, R. P.; Turner, P. C. In *Continuing Studies on Direct Aqueous Mineral Carbonation for CO2 Sequestration*, The Proceedings of the 27th International Technical Conference on Coal Utilization & Fuel Systems, 2002; 2002; pp 819-830.
6. Park, A.-H. A.; Jadhav, R.; Fan, L.-S., "CO2 Mineral Sequestration: Chemically Enhanced Aqueous Carbonation of Serpentine." *Canadian Journal of Chemical Engineering* 2003, 81, (3-4), 885-890.
7. Park, A.-H. A.; Fan, L.-S., "CO2 Mineral Sequestration: Physically Activated Aqueous Carbonation of Serpentine and pH Swing process." *Chemical Engineering Science* 2004, 59, 5241-5247.
8. O'Connor, W.K., Dahlin, D.C., Rush, G.E., Gerdemann, S.J., and Nilsen, D.N. (2004) Final report: Aqueous mineral carbonation, DOE/ARC-TR-04-002: Albany, OR, Office of Process Development, Albany Research Center, Office of Fossil Energy, US DOE, p. 21 pages plus appendices.
9. Chizmeshya, A. V. G., M. J. McKelvy, K. Squires, R. W. Carpenter, and H. Béarat (2007). A novel approach to mineral carbonation: Enhancing carbonation while avoiding mineral pretreatment process cost. DOE Final Report 924162, p.29 plus appendices, Arizona State University.
10. Welch, S., and Ullman, W., "The effect of organic acids on plagioclase dissolution rates and stoichiometry," *Geochimica et Cosmochimica ACTA*, 1993, *57* (12), 2725-2736.
11. Vandevivere, P., Welch, S., Ullman, W., and Kirchman, D., "Enhanced dissolution of silicate minerals by bacteria at near-neutral pH," *Microbial Ecology*, 1994, *27* (3), 241-251.
12. Ezenekwe, I., K. Chandran, L. A. Carrio, K. Gopalakrishnan, J. Anderson and B. Stinson, 2002. A novel application of acid-phase digestion for concurrent scod recovery and filament destruction in froth. WEFTEC 2002, Chicago, IL.

13. Stryer, Lubert (1995). Biochemistry (fourth ed.). New York - Basingstoke: W. H. Freeman and Company.
14. W. Gujer and A. J. B. Zehnder. (1983) “Conversion Process in Anaerobic Digestion,” Wat. Sci. Tech.
15. Gustafsson, J. P., “Visual MINTEQ ver 2.23,” http://www.lwr.kth.se/English/OurSoftware/vminteq/, 2004.
16. Thomas E. Furia (1972). CRC Handbook of Food Additives (2nd ed.).
17. Hanchen, M., Prigiobbe, V., et al. (2006) “Dissolution kinetics of forsteritic olivine at 90-150^{o}C including effects of the pressure of CO_2,” Geochimica et Cosmochimica Acta.
18. Brady P.V. and Walther J.V. (1990) “Olivine dissolution at 25°C: Effects of pH, CO2 and organic acids,” Geochimica et Cosmochimica Acta.
19. Samuel C.M.Krevor and KlausS.Lackner. (2011) “Enhancing serpentine dissolution kinetics for mineral carbon dioxide sequestration,” International Journal of Greenhouse Gas Control.
20. A.-H. A. Park, H. Zhao & N. Dadap. (2010) “Tailored Synthesis of Precipitated Magnesium Carbonates as Carbon-Neutral Filler Materials during Carbon Mineral Sequestration,” Fluidization XIII: New Paradigm in Fluidization Engineering.
21. Noller Herbert. “An Analysis of Energy Production Costs from Anaerobic Digestion Systems on U.S. Livestock Production Facilities,” Technical Note No. 1, October 2007.
22. S. Renou; J.G. Givaudan; S. Poulain; F. Dirassouyan; P. Moulin (2008). “Landfill leachate treatment: Review and opportunity,” Journal of Hazardous Materials. Vol.150, pp. 468–493.
23. Kristi Moriarty. “Feasibility Study of Anaerobic Digestion of Food Waste in St. Bernard, Louisiana,” Technical Report. NREL/TP-7A30-57082. Contract No. DE-AC36-08GO28308.
24. Y. Fan, H. Li1, G. Miguez-Macho (2013). “Global Patterns of Groundwater Table Depth,” Science, Vol. 339 no. 6122 pp. 940-943.
25. http://www.icispricing.com/il_shared/Samples/SubPage167.asp
26. E.R. Vieitez and S. Ghosh (1999). “Biogasification of solid wastes by two-phase anaerobic fermentation,” Biomass and Bioenergy. Vol. 16, pp 299-309.
27. Minh Tho Nguyen , Debasis Sengupta , Greet Raspoet , Luc G. Vanquickenborne (1995). “Theoretical Study of the Thermal Decomposition of Acetic Acid: Decarboxylation Versus Dehydration,” J. Phys. Chem., 99 (31), pp 11883–11888.

Technology Transfer Activities

Publication

- G. Gadikota, E. J. Swanson, H. Zhao & **A.-H. A. Park***, "Experimental Design and Data Analyses for Accurate Estimation of Reaction Kinetics and Conversion for Carbon Mineralization," *Journal of Chemical & Engineering Data* (in review).
- H. Zhao, J. Wang & **A.-H. A. Park***, "Effect of Various Chemical Additives for Enhancing Serpentine Dissolution during Carbon Storage," *Energy & Environmental Science* (in review)
- H. Zhao, Y. Park & **A.-H. A. Park***, "Effects of Volatile Fatty Acids on Antigorite Dissolution Kinetics and Ex-situ and In-situ Formation of Magnesium Carbonates," *Energy & Environmental Science* (in review)

Presentations

- E. Swanson, H. Zhao, G. Gadikota and **A.-H. A. Park**, "Accelerated Carbonation of Silicate Minerals for Safe and Permanent Storage of Anthropogenic CO_2," 2012 Society of Mining, Metallurgy & Exploration Annual Meeting, Denver, CO, Feb. 24-27, 2013.
- H. Zhao, E. Taher Sr., K. Chandran & **A.-H. A. Park**, "Kinetic and Mechanistic Studies of Microbial and Chemical Enhancement of Carbon Mineralization," AIChE annual meeting, Pittsburgh, PA, October 28 – Nov. 1, 2012.
- **A.-H. A. Park**, H. Zhao, J. Matter and K. Chandran, "Microbial and Chemical Enhancement of In-Situ Carbon Mineralization in Geological Formations," U.S. DOE Carbon Storage R&D Project Review Meeting: Developing the Technologies and Building the Infrastructure for CCUS, Pittsburgh, PA, August 21-23, 2012.
- G. Gadikota, H. Zhao and E. Swanson and **A.-H. A. Park**, "National and Engineered Carbon Mineralization in Geologic Formations for Permanent Storage of CO_2," U.S. DOE Carbon Storage R&D Project Review Meeting: Developing the Technologies and Building the Infrastructure for CCUS, Pittsburgh, PA, August 21-23, 2012. – poster presentation
- **A.-H. A. Park** & H. Zhao, "Microbial and Chemical Enhancement of Carbon Mineralization," ACEME10: Accelerated Carbonation for Environmental and Materials Engineering, Turku, Finland, November 29 – December 1, 2010.
- H. Zhao & **A.-H. A. Park**, "Kinetic and Mechanistic Studies of Chemical Enhancement of Carbon Mineralization," AIChE annual meeting," Salt Lake City, UT, November 7-12, 2010.
- **A.-H. A. Park**, H. Zhao & N. Dadap, "Tailored Synthesis of Precipitated Magnesium Carbonates as Carbon-Neutral Filler Materials during Carbon Mineral Sequestration," Fluidization XIII: New Paradigm in Fluidization Engineering, Gyeong-Ju, Korea, May 16-19, 2010.

- **A.-H. A. Park**, & H. Zhao, "Carbon Mineral Sequestration," Society of Mining, Metallurgy & Exploration Annual Meeting, Phoenix, AZ, February 28 – March 3, 2010.

Invited Lectures given by Park that included the findings from this project

- Invited talk on Research Coordination Network on Carbon Capture, Utilization and Storage, 2013 Carbon Management Technology Conference, Alexandria, VA (October 21, 2013).
- Invited talk at the ACS National Meeting, the session titled "Materials and Technologies for CO_2 Capture, Sequestration, and Conversion," Indianapolis, IN (September 8-12, 2013).
- Keynote lecture, the Ann. Conference on Steel Making, POSCO, Pohang, Korea (Aug. 20, 2013).
- Invited seminar at Hyundai Heavy Industry, Ulsan, Korea (August 13, 2013).
- Invited talk at the 12th International Conference on Carbon Dioxide Utilization (ICCDU XII), Washington DC (June 23-27, 2013).
- Department of Chemical Engineering, Princeton University (April 3rd, 2013).
- Department of Chemistry, City College of New York (March 18th, 2013).
- Department of Chemical Engineering, Illinois Institute of Technology (March 6th, 2013).
- Geology, Earth Science and Oceanography (GEOS) Series, City University of New York, New York, NY (Feb. 22nd, 2013).
- Invited speaker for the ULTRA (Universal Linkage for Top Research Advice) program by the Korean Ministry of Education, Science & Technology, Seoul, Korea (December 13th, 2012).
- Department of Chemical Engineering, New Jersey Institute of Technology (December 10th, 2012).
- Department of Chemical Engineering, UC Berkeley (November 28th, 2012).
- Keynote lecture at the 2012 International Forum on Accelerated Weathering and Carbonation for Mineral Sequestration, Taipei, Taiwan (November 6th, 2012).
- Invited seminar at ExxonMobil Research and Engineering Company, Annandale, NJ (October 25th, 2012).
- Invited talk at Pacific Northwest National Laboratory, Richland, WA (October 15th, 2012).
- Invited speaker for the ULTRA (Universal Linkage for Top Research Advice) program by the Korean Ministry of Education, Science & Technology, Los Angeles, CA (August 9th, 2012).

- Department of Materials Science & Engineering, Stony Brook University (July 18th, 2012).
- Invited talk at the symposium titled "Green Chemistry in Energy and Fuels": **A.-H. A. Park**, "Towards Sustainable Energy: Carbon Capture, Utilization and Storage (CCUS)," ACS National Meeting, Philadelphia, PA (August 19-23, 2012).
- Invited talk at Capital District E-Week (Chemical Engineering Track), Albany, NY (February 16-17, 2012).
- Invited talk at the 6th Sino-US Joint Conference of Chemical Engineering, Beijing, China (Nov. 7-10, 2011).
- Invited talk at the Korean Institute of Geoscience and Mineral Resources (KIGAM) workshop, Jeju Island, Korea (November 3-4, 2011).
- Invited lecture at the Korean Mission to the UN (April 11, 2011).
- Invited lecture at the New York Metro Chapter Seminar of KSEA, New York, NY (Feb. 11, 2011).
- Department of Chemical and Biological Engineering, Northwestern University (January 27, 2011).
- Plenary lecture at the 3rd US-China Symposium on CO_2 Emission Control Science & Technology in Hangzhou, Zhejiang, China (December 10-12, 2010).
- Environmental Engineering, Department of Civil Engineering, University of Rome "Tor Vergata" in Italy (December 3, 2010).
- Keynote lecture at ACEME10: Accelerated Carbonation for Environmental and Materials Engineering, Turku, Finland (November 29-December 1, 2010).
- Department of Mechanical Engineering, New Jersey Institute of Technology (October 13, 2010).
- Invited Lecture at the University of Delaware Energy & Sustainability 2010 conference (September 23, 2010).
- Invited Seminar at Specialty Minerals Inc., Bethlehem, PA (June 2, 2010).
- Invited Seminar at the Research Institute of Industrial Science & Technology (RIST) owned by the Pohang Iron and Steel Company (May 18, 2010).
- Department of Chemical and Biochemical Engineering, Rutgers, The State University of New Jersey (April 28, 2010).
- Invited talk at the Lenfest Foundation, Bethlehem, PA (April 20, 2010).
- Invited talk at the AIChE New Haven Section (April 6, 2010).
- Invited talk at the 6th Chemical Engineering Conference for Collaborative Research in Eastern Mediterranean Countries (EMCC6), Antalya, Turkey (March 7-12, 2010).
- Department of Chemical Engineering, the City College of New York (February 1, 2010).

Schedule/Milestone Status

Task/ Subtask#	Tasks	Year I				Year II				Year III			
		Qt1	Qt2	Qt3	Qt4	Qt1	Qt2	Qt3	Qt4	Qt1	Qt2	Qt3	Qt4
1.0	**Project Management, Planning, and Reporting**												
1.1	Project Management Plan												
1.2	Reporting and Budgets												
1.3	Presentation and Briefings												
	Final Report Preparation												
2.0	**Characterization of minerals and thermodynamic modeling of CO_2-mineral-brine systems with potential organic acids (Phase I)**												
2.1	Mineral characterization												
2.2	Thermodynamic modeling												
3.0	**Development of a microbial system for the production of volatile fatty-acids from organic waste streams (Phase II)**												
3.1	Fermentation of organic waste streams for volatile fatty-acid production												
3.2	Investigation of microbial ecology of acidogenic fermentation												
4.0	**Kinetic and mechanistic studies of chemical enhancement of mineral dissolution and carbonation using organic acids (Phase III)**												
4.1	Design and fabrication of a high pressure reactor												
4.2	Kinetic and mechanistic studies of mineral dissolution and carbonation												
4.3	Characterization of mineral carbonates												
5.0	**Environmental and economic assessments (Phase IV)**												